

1 **SUPPLEMENTAL INFORMATION: SEMPLE ET AL.**

2 ¹

3 1. NEWLY DOCUMENTED DEFORMATION NOT ALREADY INCLUDED IN MAIN TEXT

4 Contents

- 5 (1) Table S1: Sites of suspected anthropogenic deformation and the potential
6 origin
- 7 (2) References
- 8 (3) Figure S1: Interferogram showing deformation in Antelope Valley, CA with
9 nearby cGPS
- 10 (4) Figure S2: Interferogram showing deformation in Coso, CA with nearby cGPS
- 11 (5) Figure S3: Interferogram showing deformation in Las Vegas, NV with nearby
12 cGPS
- 13 (6) Figure S4: Interferogram showing deformation near East Mesa, CA with
14 nearby cGPS
- 15 (7) Figure S6: Interferogram showing deformation near Salt Lake City, UT with
16 nearby cGPS
- 17 (8) Figure S5: Interferogram showing deformation in Escalante Valley, UT with
18 nearby cGPS
- 19 (9) Figure S7: Interferogram showing deformation in Livingston County, NY
- 20 (10) Figure S8: Interferogram showing deformation in southwestern PA and north-
21 ern WV, with nearby cGPS
- 22 (11) Figure S9: Interferogram showing deformation near Amboy, CA

¹Title: An incomplete inventory of suspected human-induced surface deformation in North America detected by satellite Interferometric Synthetic Aperture Radar

- 23 (12) Figure S10: Interferogram showing deformation in Tuscaloosa County, AL
24 (13) Figure S11: Interferogram showing deformation in the Central Valley, CA
25 (14) Figure S12: Interferogram showing deformation Round Mountain Mine
26 (15) Figure S13: Interferogram showing deformation Palm Tree Farm, CA
27 (16) Figure S14: Interferogram showing deformation Quinn River Valley, NV.
28 (17) Figure S15: Interferogram showing deformation San Simon, NM.
29 (18) Figure S16: Interferogram showing deformation Silver State Valley, NV
30 (19) Figure S17: Interferogram showing deformation US Borax Mine, CA
31 (20) Figure S18: Interferogram showing deformation Kennecott, UT
32 (21) Figure S19: Interferogram showing deformation Kings River Valley, NV
33 (22) Figure S20: Interferogram showing deformation Little Salt Lake, UT
34 (23) Figure S21: Interferogram showing deformation Mesquite Mine, CA
35 (24) Figure S22: Interferogram showing deformation Little America, WY
36 (25) Figure S23: Interferogram showing deformation near Beaver, UT
37 (26) Figure S24: Interferogram showing deformation North and South Paradise
38 Valley, NV
39 (27) Figure S25: Interferogram showing deformation Nuevo Delicias, Mexico
40 (28) Figure S26: Interferogram showing deformation DMAD Reservoir, UT
41 (29) Figure S27: Interferogram showing deformation Elko, NV
42 (30) Figure S28: Interferogram showing deformation East Los Trios, Mexico
43 (31) Figure S29: Interferogram showing deformation east Osgood Mountain, NV
44 (32) Figure S30: Interferogram showing deformation south Flowell, UT
45 (33) Figure S31: Interferogram showing deformation Fields west of Utah Lake,
46 UT
47 (34) Figure S32: Interferogram showing deformation Grass Valley, NV
48 (35) Figure S33: Interferogram showing deformation Jesus Garcia, Mexico

- 49 (36) Figure S34: Interferogram showing deformation South Espia and Asension,
 50 Mexico
- 51 (37) Figure S35: Interferogram showing deformation Oreana, ID
- 52 (38) Figure S36: Interferogram showing deformation Goldstrike, NV
- 53 (39) Figure S37: Interferogram showing deformation south Lake Los Angeles, CA
- 54 (40) Figure S38: Interferogram showing deformation Centennial, CO
- 55 (41) Figure S39: Interferogram showing deformation Chemetall Foote Lithium
 56 Operation, CA
- 57 (42) Figure S40: Interferogram showing deformation Corcoran, CA
- 58 (43) Figure S41: Interferogram showing deformation Corona, CA
- 59 (44) Figure S42: Interferogram showing deformation Crane, OR
- 60 (45) Figure S43: Interferogram showing deformation Deming, NM

SUPPLEMENTAL TABLE 1

Name/Location	InSAR ² track/path	Reference and/or Figure	Lat/Long ³
---------------	----------------------------------	----------------------------	-----------------------

Groundwater

Raft River, ID	84, 356	Figure 9; <i>Lofgren</i> (1975)	42.2 -113.32
Near Oreana, ID	213	Figure S35	43.04 -116.38
Near Burley, ID	84	Figure 8	42.38 -114.02
Escalante Valley, UT	84, 356?	Figure S5; <i>Forster</i> (2006); <i>Lund et al.</i> (2005)	37.71 -113.66
Salt Lake City, UT	41	Figure S6	40.67 -111.96
Near Beaver, UT	41	Figure S23	38.26 -112.72
Roswell, NM	12, 284?	Figure 3	33.17 -104.35
Nuevo Delicias, Mexico	284	Figure S25	29 -106.27
E. of Los Trios, Chih., Mexico	98	Figure S28	31.45 -107.57
Jesus Garcia, Sonora, Mexico	227	Figure S33	30.76 -112.44

²All InSAR are from ERS and Envisat unless otherwise noted³Location refers to approximate center of deformation

North Paradise Valley, NV	213	Figure S24	41.47 -117.53
South Paradise Valley, NV	213	Figure S24	41.19 -117.65
Ag. Fields S. of Goldstrike, NV	213	Figure S36	40.87 -116.48
Ag. Fields E. of Osgood Mts, NV	213	Figure S29	41.11 -117.21
Near Desert Center Airport, CA	84, 356?	Figure S13	33.711 -115.252
Ag. Fields S. of Lake LA, CA	442	Figure S37	34.57 -117.84
Rogers Dry Lake (Edwards AFB)	442	<i>Sneed et al. (2006)</i>	34.95 -117.86
Reese River Valley, NV	442	<i>Gourmelen et al. (2007)</i>	40.4 -117.1
Diamond Valley, NV	399, 170?	<i>Gourmelen et al. (2007); Arai (2009); Greene (2014)</i>	39.7 -116
Antelope Valley, NV	213, 442	<i>Casu et al. (2008); Gourmelen et al. (2007)</i>	40.03 -117.29
Quinn River Valley, NV	213, 442?	Figure S14; <i>Greene (2014)</i>	41.55 -117.82
Silver State Valley, NV	213, 442?	Figure S16	41.19 -117.87
Elko, NV	399	Figure S27	40.86 -115.73
Grass Valley, NV	213	Figure S32	40.74 -117.75
Fish Lake Valley, NV/CA	213, 442	<i>Gourmelen et al. (2010, but not discussed)</i>	37.53 -117.93
Tonopah, AZ	270	Figures 10-11:	33.6 -113.2
Knights Landing, CA		<i>Blodgett et al. (1990)</i>	38.8 -121.78
Arbuckle, CA		<i>Blodgett et al. (1990)</i>	39 -122.05
Davis, CA		<i>Blodgett et al. (1990)</i>	38.54 -121.74
Byron, CA		<i>Blodgett et al. (1990)</i>	37.92 -121.53
Stockton, CA		<i>Blodgett et al. (1990)</i>	37.96 -121.29
Woodland, CA		<i>Ikehara (1994)</i>	38.69 -121.78
San Joaquin Valley, CA		<i>Sneed et al. (2013)</i>	37.06 -120.33
Cantua Creek, CA		<i>Ireland et al. (1984)</i>	36.44 -120.32
Firebaugh, CA		<i>Ireland et al. (1984)</i>	36.66 -120.52
Huron, CA		<i>Ireland et al. (1984)</i>	36.19 -120.13
Pixley, CA	485	<i>Ireland et al. (1984)</i>	35.97 -119.29
Near Kern Lake, CA		<i>Ireland et al. (1984)</i>	35.14 -119.02
Paso Robles, CA:		<i>Valentine et al. (2000)</i>	35.7 -120.66

Atascadero, CA		<i>Valentine et al. (2000)</i>	35.52 -120.64
Red Hills, CA		<i>Valentine et al. (2000)</i>	35.57 -120.3
Shandon, CA		<i>Valentine et al. (2000)</i>	35.62 -120.37
Antelope Valley, CA	442	Figure S1; <i>Galloway et al. (1998)</i>	34.92 -118.29
Antelope Valley, CA (second lobe)	442	Figure S1 <i>Galloway et al. (1998)</i>	34.8 -118
Corona, CA	399	Figure S41	33.91 -117.59
Palm Desert, CA		<i>Sneed and Brandt (2013)</i>	33.74 -116.38
Indian Wells, CA		<i>Sneed and Brandt (2013)</i>	33.72 -116.34
La Quinta, CA		<i>Sneed and Brandt (2013)</i>	33.65 -116.27
Mirage Lake, CA		<i>Sneed and Brandt (2013); Sneed et al. (2003)</i>	34.59 -117.56
Harper Lake, CA		<i>Sneed et al. (2003)</i>	35.02 -117.19
Fields S. of Flowell, UT	41	Figure S30	38.87 -112.43
Bicycle Lake, Fort Irwin, CA		<i>Densmore et al. (2010)</i>	35.28 -116.63
Truckee, CA		<i>Bell et al. (2008)</i>	39.36 -120.14
Truckee Meadows (Reno), NV		<i>Bell et al. (2008)</i>	39.53 -119.77
Chalk Hills, NV		<i>Bell et al. (2008)</i>	39.52 -119.88
Fields near Beckwourth, CA	299	<i>Bell et al. (2008)</i>	39.79 -120.22
Cold Springs Valley, NV		<i>Bell et al. (2008)</i>	39.68 -120
Warm Springs Valley, NV		<i>Bell et al. (2008)</i>	39.82 -119.65
Lemmon Valley, NV		<i>Bell et al. (2008)</i>	39.67 -119.86
Corcoran, CA	256, 485	Figures S40, S11; <i>Farr (2016)</i>	36.15 -119.57
Carson City, NV	256	<i>Bell et al. (2008)</i>	39.18 -119.76
Near Honey Lake, CA		<i>Bell et al. (2008)</i>	40.13 -120.23
Kings River Valley, NV	256	Figure S19; <i>Greene (2014)</i>	41.75 -118.22
Crane, OR	256	Figure S42	43.43 -118.6
Las Vegas, NV	146, 356, 84	Figure S3; <i>Amelung et al. (1999); Pavelko et al. (1999)</i>	36.25 -115.23
Parowan Valley, UT	41	<i>Forster (2006)</i>	37.9 -112.8

Cedar Valley, UT	41	<i>Knudsen et al. (2014)</i>	37.72 -113.1
Fields west of Utah Lake, UT	41	Figure S31	40.27 -112.04
Milford area, UT	41,356?	<i>Forster (2006)</i>	38.35 -113
Buckman Well field, NM	277	<i>Thomsen and Fialko (2003); Pollack et al. (2013)</i>	35.8 -106.15
Rio Rancho, NM	277	<i>Heywood et al. (2002)</i>	35.26 -106.7
Albuquerque, NM		<i>Heywood et al. (2002)</i>	35.1 -106.55
Deming, NM	98	Figure S43	32.27 -107.76
San Simon, NM	141	Figure S15	32.21 -109.166
Near El Espia, Chih., Mexico	98	Figure S34	31.27 -108
Near Asension, Chih., Mexico	98	Figure S34	31.06 -107.97
San Luis Valley, CO	98	<i>Reeves et al. (2011)</i>	37.42 -106
Near Ojai, CA		<i>Marshall et al. (2013)</i>	34.45 -119.22
El Rio (near GPS station P729)		<i>Marshall et al. (2013)</i>	34.23 -119.12
Ranegras Valley, AZ		Figure 10; <i>ADWR (2015)</i>	33.7 -113.8
McMullen Valley, AZ	270	Figure 10; <i>ADWR (2015)</i>	33.9 -113.3
Harquahala Valley, AZ		Figure 10; <i>ADWR (2015)</i>	33.5 -113.25
Gila Bend, AZ		Figure 10; <i>ADWR (2015)</i>	33 -112.7
Buckeye, AZ		<i>ADWR (2015)</i>	33.36 -112.6
West Valley, AZ	270	<i>ADWR (2015); Miller and Shirzaei (2015)</i>	33.6 -112.3
East Valley, AZ		<i>ADWR (2015); Miller and Shirzaei (2015)</i>	33.4 -111.85
Scottsdale/Phoenix, AZ	227	<i>ADWR (2015)</i>	33.65 -111.92
Maricopa Stanfield, AZ		<i>ADWR (2015)</i>	32.9 -112
Hawk Rock, AZ	227	<i>ADWR (2015)</i>	33.38 -111.6
Picacho, AZ		<i>ADWR (2015)</i>	32.75 -111.55
Tucson, AZ	184	<i>ADWR (2015)</i>	32.2 -110.95
Green Valley, AZ		<i>ADWR (2015)</i>	31.95 -110.96
Fort Grant Road, AZ	184	<i>ADWR (2015)</i>	32.3 -109.9
Kansas Settlement, AZ	184	<i>ADWR (2015)</i>	32.1 -109.8
Elfrida, AZ		<i>ADWR (2015)</i>	31.7 -109.7

Bowie San Simon, AZ		<i>ADWR</i> (2015)	32.25 -109.23
Houston, TX		<i>Buckley et al.</i> (2003)	29.86 -95.58
Mexico City, Mexico		<i>Cabral-Cano et al.</i> (2008); <i>Osmanoğlu et al.</i> (2011); <i>Chaussard et al.</i> (2014)	19.4 -99.13
Morelia, Mexico		<i>Chaussard et al.</i> (2014); <i>Cigna et al.</i> (2012)	19.7 -101.2
Queretaro, Mexico		<i>Pacheco et al.</i> (2006); <i>Arroyo et al.</i> (2002); <i>Chaussard et al.</i> (2014)	20.59 -100.39
San Luis Potosi, Mexico		<i>Mata-Segura et al.</i> (2004); <i>López-Doncel et al.</i> (2006); <i>Chaussard et al.</i> (2014)	22.16 -100.99
Villa de Arista, Mexico		<i>Chaussard et al.</i> (2014)	22.65 -100.85
Villa de Reyes, Mexico		<i>Chaussard et al.</i> (2014)	21.81 -100.94
San Luis de la Paz, Mexico		<i>Chaussard et al.</i> (2014)	21.3 -100.53
El Paredon, Mexico		<i>Chaussard et al.</i> (2014)	21.07 -100.6
Salamanca, Mexico		<i>Chaussard et al.</i> (2014)	20.58 -101.2
Celaya, Mexico		<i>Chaussard et al.</i> (2014)	20.52 -100.82
Irapuato, Mexico		<i>Chaussard et al.</i> (2014)	20.68 -101.36
Silao, Mexico		<i>Chaussard et al.</i> (2014)	20.96 -101.44
Leon, Mexico		<i>Chaussard et al.</i> (2014)	21.13 -101.68
Aguas calientes, Mexico		<i>Chaussard et al.</i> (2014)	21.9 -102.26
Luis Moya, Mexico		<i>Chaussard et al.</i> (2014)	20.72 -103.17
Guadalajara, Mexico		<i>Chaussard et al.</i> (2014)	20.72 -103.17
Tepic, Mexico		<i>Chaussard et al.</i> (2014)	21.52 -104.93
Ahuacatlan, Mexico		<i>Chaussard et al.</i> (2014)	21.06 -104.48
Zamora Hidalgo, Mexico		<i>Chaussard et al.</i> (2014)	20.05 -102.32
Puebla, Mexico		<i>Chaussard et al.</i> (2014)	19.04 -98.21
Toluca de Lerdo, Mexico		<i>Chaussard et al.</i> (2014)	19.32 -99.63
Pomona, CA		<i>Argus et al.</i> (2005); <i>Watson et al.</i> (2002)	34.05 -117.75

Santa Ana, CA		<i>Argus et al. (2005); Bawden et al. (2001); Watson et al. (2002)</i>	33.75 -118
Santa Clara Valley, CA		<i>Schmidt and Bürgmann (2003)</i>	37.36 -121.9
San Gabriel Valley, CA		<i>King et al. (2007)</i>	34.13 -118
Port of Seattle, WA		<i>Finnegan et al. (2008)</i>	47.59 -122.34
Kent, WA		<i>Finnegan et al. (2008)</i>	47.38 -122.23
Tacoma, WA		<i>Finnegan et al. (2008)</i>	47.32 -122.38
university place, WA		<i>Finnegan et al. (2008)</i>	47.2 -122.58
Vancouver, BC		<i>Mazzotti et al. (2009)</i>	49.16 -123.16
Alexandria, VA uplift	CSK	Figure 13; <i>Hoppe et al. (2016); Hsiao (2016)</i>	38.82 -77.02
near Amboy crater, CA	Envisat	Figure S9	34.49 -115.65
Near Centennial, CO	55	Figure S38	39.56 -104.7
Near Little Salt Lake, UT	41	Figure S20	37.94 -112.83
Ciudad Guzmán, Mexico		<i>Brunori et al. (2015)</i>	19.71 -103.47

Geothermal

East Mesa, CA	84	Figures 6, 7, S4; <i>Massonnet et al. (1997); Han et al. (2011)</i>	32.8 -115.27
Dixie Valley, NV	213	<i>Foxall and Vasco (2008); Greene (2014)</i>	39.98 -117.83
Raft River, ID	84, 356	Figure 9; <i>Ali et al. (2016)</i>	42.09 -113.36
Coso, CA	442, 170	Figure S2; <i>Casu et al. (2008); Fialko and Simons (2000); Wicks et al. (2001)</i>	36.03 -117.8
Desert Peak, NV	256	<i>Ali et al. (2016)</i>	39.76 -118.95
Bradys, NV	256	<i>Shevenell et al. (2012); Ali et al. (2015)</i>	39.78 -119
Long Valley, CA		<i>Tizzani et al. (2007)</i>	37.64 -118.85

Cerro Prieto, Mexico	84, 306	<i>Carnec and Fabriol</i> (1999); <i>Sarychikhina et al.</i> (2011)	32.37 -115.24
Soda Lakes, NV		<i>Tibuleac and Eneva</i> (2011)	39.53 -118.88
Geysers, CA		<i>Vasco et al.</i> (2013)	38.8 -122.78
Heber, CA?	84	<i>Eneva et al.</i> (2012)	32.72 -115.5
Salton Sea, CA	84, 356, 306	<i>Eneva et al.</i> (2012)	33.16422933 -115.6144738
Steamboat Springs	256	<i>Bell et al.</i> (2008)	39.388 -119.743
Stillwater, NV		<i>Hammond and Bell</i> (2013)	39.545 -118.557
San Emidio, NV		<i>Eneva et al.</i> (2011)	40.38 -119.4
Amedee, CA		<i>Bell et al.</i> (2008)	40.37 -120.26

Mining

Amethyst Sage Mine, NV		<i>Greene</i> (2014)	41.616 -118.343
McCoy-Cove Mine, NV		<i>Greene</i> (2014)	40.336 -117.201
Twin Creeks mine, NV	213	<i>Katzenstein</i> (2008); <i>Greene</i> (2014)	41.26 -117.16
Lone Tree gold mine, NV	213, 442	<i>Casu et al.</i> (2008); <i>Greene</i> (2014)	40.83 -117.2
Cortez gold mine, NV	442, 170?	<i>Casu et al.</i> (2008); <i>Gourmelen et al.</i> (2007); <i>Greene</i> (2014)	40.25 -116.7
Carlin/Gold Quarry mine, NV	442	<i>Greene</i> (2014)	40.78 -116.2
Dexter (Betze-Post) mine, NV	442	<i>Gourmelen et al.</i> (2007); <i>Greene</i> (2014)	40.97 -116.37
Round Mountain mine, NV	442	Figure S12	38.7 -117.09
Chemetall Foote Lithium Operation, Silver Peak, CA	442	Figure S39	37.78 -117.57
U.S. Borax Boron mine, CA	442	Figure S17	35.05 -117.69
Mining near Little America, WY	227	<i>Coyne</i> (1988); Figure S22	41.49 -109.77
IPP coal power plant, UT	41		39.52 -112.6
Crandell Canyon Mine collapse, UT		(<i>Plattner et al.</i> , 2010)	39.465 -111.22
west ridge mine, UT		<i>Ismaya and Donovan</i> (2012)	39.63 -110.4
deer creek mine, UT		<i>Donovan et al.</i> (2010)	39.4 -111.1

dugout canyon mine, UT		<i>Donovan et al. (2010)</i>	39.68 -110.55
Mesquite Mine, CA	84	Figure S21	33.056 -114.98
Kennecott Tailings Pond, UT	41	Figure S18	40.73 -112.12
Centralia Coal Mine, WA		<i>Prush and Lohman (2015)</i>	46.773333 -122.843333
Near Rice Lake, Saskatchewan		<i>Samsonov et al. (2014)</i>	52.04 252.88
Near Rice Lake, Saskatchewan		<i>Samsonov et al. (2014)</i>	52.12 253.025
Near Rice Lake, Saskatchewan		<i>Samsonov et al. (2013)</i>	52.13 253.16
Livingston County, NY	p137, p138	Figure S7; <i>Valentino (2016)</i>	42.74 -77.8
coal mine PA	p143	Figure S8	40.03 -80.32
coal mine PA	p143	Figure S8	39.85 -80.106
coal mines PA/WV	p143	Figure S8	39.87 -80.46
coal mines PA	p143	Figure S8	39.8 -80.08
coal mine WV	p143	Figure S8	39.66 -80.21
coal mine WV	p143	Figure S8	39.58 -80.37
coal mine WV	p143	Figure S8	39.5 -80.45
coal mine PA	p143	Figure S8	39.78 -80.3
coal mine WV	p143	Figure S8	39.8 -80.62
coal mine WV	p143	Figure S8	39.775 -80.632
coal mine WV	p143	Figure S8	39.642 -80.243
coal mine WV	p143	Figure S8	39.651 -80.321
coal mine Tuscaloosa county, AL	p159	Figure S10	33.366 -87.268
coal mine Tuscaloosa county, AL	p159	Figure S10	33.372 -87.347
coal mine Tuscaloosa county, AL	p159	Figure S10	33.299 -87.245
coal mine Tuscaloosa county, AL	p159	Figure S10	33.505 -87.303
coal mine Tuscaloosa county, AL	p159	Figure S10	33.338 -87.197
near Frank landslide, Alberta		<i>Mei et al. (2008)</i>	49.59 -114.4
Near Estevan, Saskatchewan		<i>Samsonov et al. (2015)</i>	49.09 -103.05
Bayou corn sinkhole, LA		<i>Jones and Blom (2014)</i>	30.01 -91.14
Springfield, IL coal mines		<i>Grzovic and Ghulam (2015)</i>	39.82 -89.62
Meikle-Goldstrike Mine		<i>Greene (2014)</i>	41.159 -116.004
Florida Canyon Mine		<i>Greene (2014)</i>	40.578 -118.238
Thomas Canyon Pit		<i>Greene (2014)</i>	40.96 -117.74

Moltan Mine and Fernley Plant		<i>Greene</i> (2014)	39.828 -118.969
Fallon Plant		<i>Greene</i> (2014)	39.505 -118.912
Popcorn Mine and Plant		<i>Greene</i> (2014)	39.474 -118.777
Ruby Hill Mine		<i>Greene</i> (2014)	39.554 -115.988
Four Clover Mine		<i>Greene</i> (2014)	38.888 -119.439
Nevada Works Mine		<i>Greene</i> (2014)	38.87 -117.897
Silver Peak Mine		<i>Greene</i> (2014)	37.767 -117.583
Yerington Plant		<i>Greene</i> (2014)	38.939 -119.19

Hydrocarbon

Jonah Field (subsidence 1), WY	270	Figure 12	42.7 -109.81
Jonah Field (subsidence 2), WY	270	Figure 12	42.54 -109.66
Jonah Field (uplift), WY	270	Figure 12	42.57 -109.83
Elk Hills Oil Field, CA	213	<i>Wynn</i> (2003)	35.27 -119.43
Oildale, CA	213, 485	Figure S11; <i>Snieder et al.</i> (2007)	35.45 -119
Lost Hills, CA	256, 163?	<i>Fielding et al.</i> (1998)	35.6 -119.7
Stevens, CA	485	Figure S11	35.31 -119.1877
Missouri Triangle, CA	485	Figure S11	35.45 -119.715
Near Tupman, CA	485	Figure S11	35.302 -119.293
Near Reward, CA	485	Figure S11	35.35 -119.66
Near Derby Acres, CA	485	Figure S11	35.238 -119.60
Near Reef Station, CA	485	Figure S11	35.89 -120.022
Beverly Hills oil field, CA		<i>Argus et al.</i> (2005)	34.056289 -118.37559
Las Cienegas oil field, CA		<i>Argus et al.</i> (2005)	34.04771338 -118.3406144
Downtown Los Angeles oil field, CA		<i>Argus et al.</i> (2005)	34.03680421 -118.2613694
East Los Angeles oil field, CA		<i>Argus et al.</i> (2005)	33.999853 -118.143712
Montebello oil field, CA		<i>Argus et al.</i> (2005)	34.02652187 -118.1096756
Whittier oil field, CA		<i>Argus et al.</i> (2005)	33.99434751 -118.041362
Santa Fe springs, CA		<i>Argus et al.</i> (2005)	33.93956269 -118.0710048
West Coyote oil field, CA		<i>Argus et al.</i> (2005)	33.90944923 -117.9765168
Inglewood oil field, CA		<i>Argus et al.</i> (2005)	33.99864685 -118.3675815
Long Beach oil field, CA		<i>Argus et al.</i> (2005)	33.801991 -118.173279

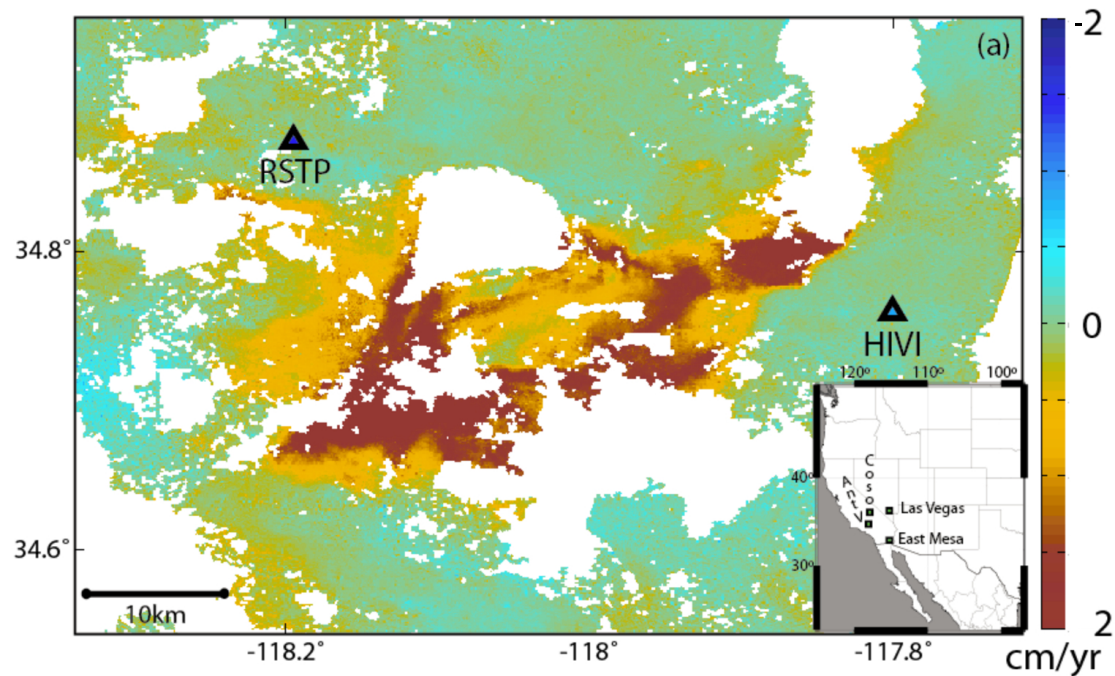
Huntington beach oil field, CA		<i>Argus et al. (2005)</i>	33.67019795 -118.0118929
Torrance oil field, CA		<i>Argus et al. (2005)</i>	33.846148 -118.394165
Wilmington oil field, CA		<i>Argus et al. (2005); Bawden et al. (2001)</i>	33.74235727 -118.190357
Powder River Basin coalbed methane, WY		<i>Grigg and Katzenstein (2013); Semmens (2012)</i>	44 -106
Ventura, CA (near GPS station VNCO)		<i>Marshall et al. (2013)</i>	34.31 -119.31
Maricopa, CA		<i>Marshall et al. (2013)</i>	35.08 -119.38
South of Bakersfield, CA		<i>Marshall et al. (2013)</i>	35.05 -119.1
Cold Lake heavy oil field, Alberta		<i>Stancliffe and van der Kooij (2001)</i>	55.07 -110.87
Hangingstone injection, Alberta		<i>Khakim et al. (2013)</i>	56.32 -111.645
Scurry County, west Texas;		<i>Yang et al. (2015)</i>	32.75 -101
<i>CO</i> ₂ injection, South Texas		<i>Karegar et al. (2015)</i>	29 -95.5
Primrose cyclic steam stimulation, Alberta		<i>Baek et al. (2015)</i>	54.83 -110.53
Athabasca, Alberta: Surmont		<i>Pearse et al. (2014)</i>	56.2 -110.98
Athabasca, Alberta: Long Lake		<i>Pearse et al. (2014)</i>	56.41 -110.97
Athabasca, Alberta: MacKay River		<i>Pearse et al. (2014)</i>	57.2 -111.9
Athabasca, Alberta: Firebag		<i>Pearse et al. (2014)</i>	57.22 -110.88
Cranfield, MS		<i>Zhao et al. (2012)</i>	31.5 -91.3
Cranfield, MS		<i>Zhao et al. (2012)</i>	32 -91.7
Salt Creek, WY		<i>Zhao et al. (2012)</i>	43.7 -106
Salt Creek, WY		<i>Zhao et al. (2012)</i>	43.4 -106.3
Farnham dome, UT		<i>Zhao et al. (2012)</i>	39.6 -110.9
Raton Basin, CO ⁴		<i>Barnhart et al. (2014)</i>	37.48 -104.67
Raton Basin, NM		<i>Barnhart et al. (2014)</i>	36.79 -104.49
Raton Basin, NM		<i>Barnhart et al. (2014)</i>	37.02 -104.97
Raton Basin, NM		<i>Barnhart et al. (2014)</i>	36.92 -105.16

⁴Any sites in the Raton Basin listed here could be cause by groundwater pumping (*Barnhart et al., 2014*)

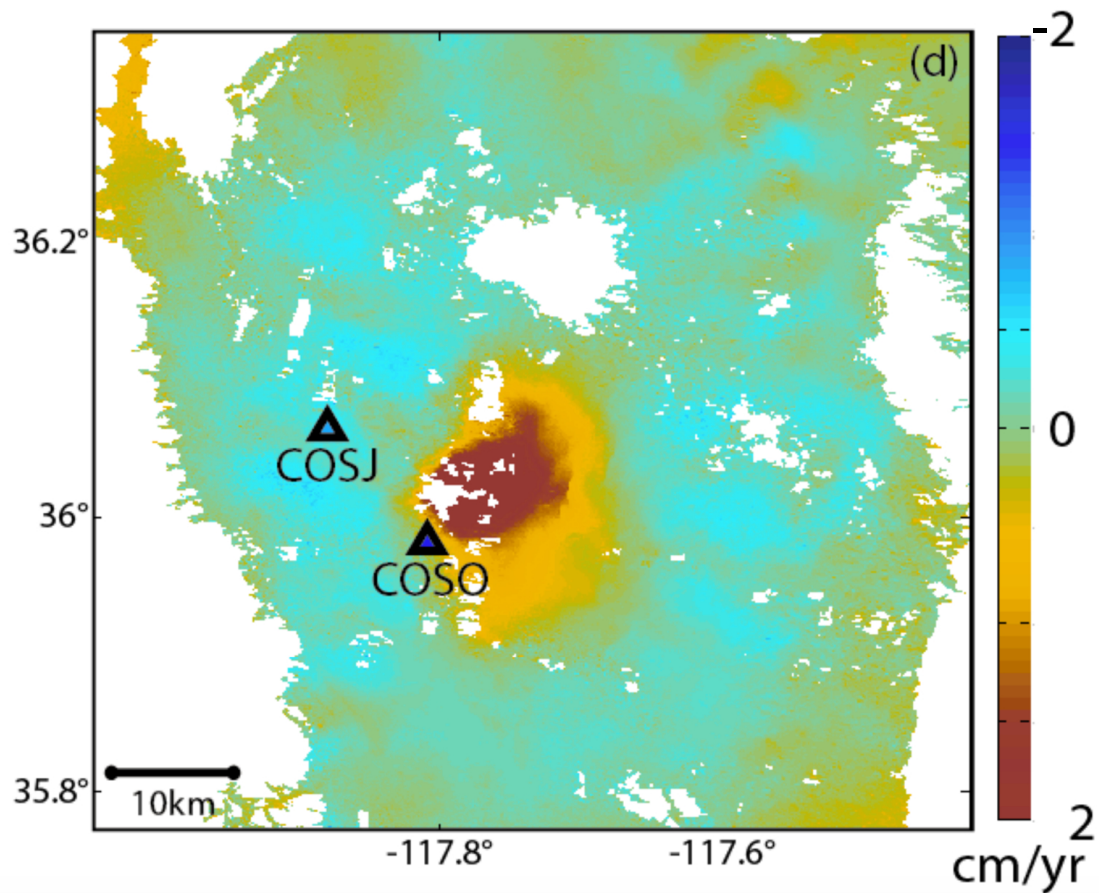
Rusk County, TX		Figures 16 & 17	32.099481 -94.729917
Rusk County, TX		Figure 16	32.009333 -94.662850
Rusk County, TX		Figure 16	32.045721 -94.686063
Panola County, TX		Figure 16	32.129250 -94.558478

Other

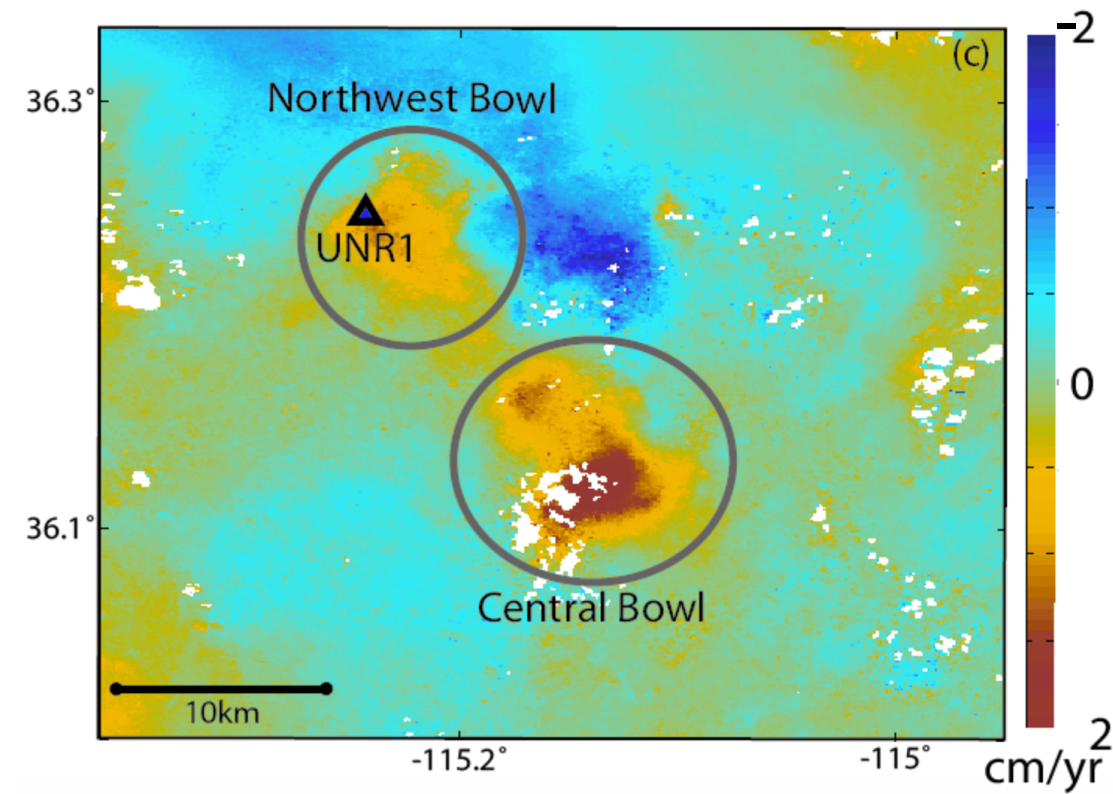
Lake Mead, NV	84	<i>Cavalié et al. (2007)</i>	36.13 -114.44
Nevada Test Site	399	<i>Vincent et al. (2003).</i>	37 -116
New Orleans, LA		<i>Dixon et al. (2006)</i>	29.96 -90.08
Near Moorpark, CA		<i>Marshall et al. (2013)</i>	34.3 -118.92
DMAD Reservoir, UT	41	Figure S26	39.43 -112.44
Washington, D.C. subsidence	CSK	Figure 13; <i>Hoppe et al. (2016); Hsiao (2016)</i>	38.89 -76.97
Craney Island, VA		<i>Bekaert et al. (2017)</i>	36.923 -76.357
Naval Shipyard, VA		<i>Bekaert et al. (2017)</i>	36.816 -76.2995
Island for Monitor Merrimack Bridge, VA		<i>Bekaert et al. (2017)</i>	36.946 -76.404



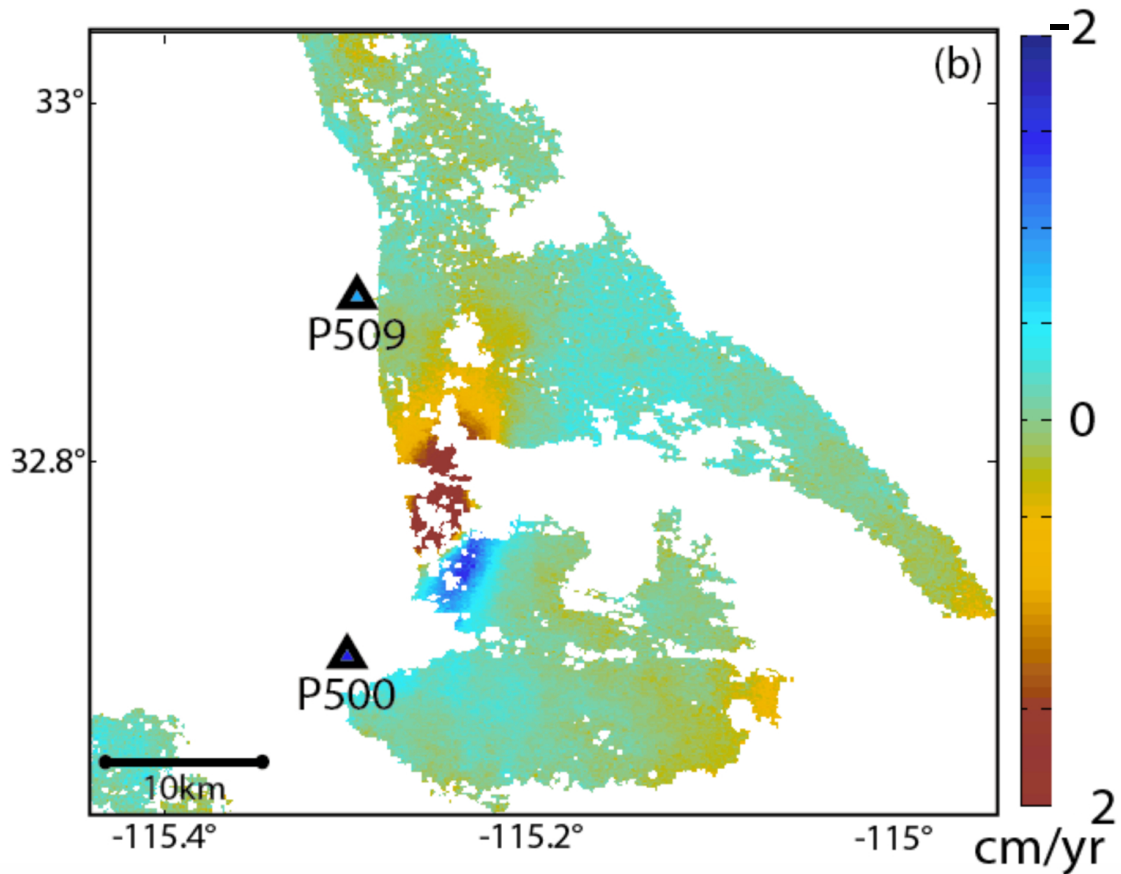
SUPPLEMENTAL FIGURE 1. Unwrapped interferogram at Antelope Valley, CA from Envisat 24 Nov. 2005-3 Dec. 2009 with insert map showing the location of this figure (labeled "AntV") and sites in the next 3 figures. Continuous GPS stations are shown as triangles with the four character station id code.



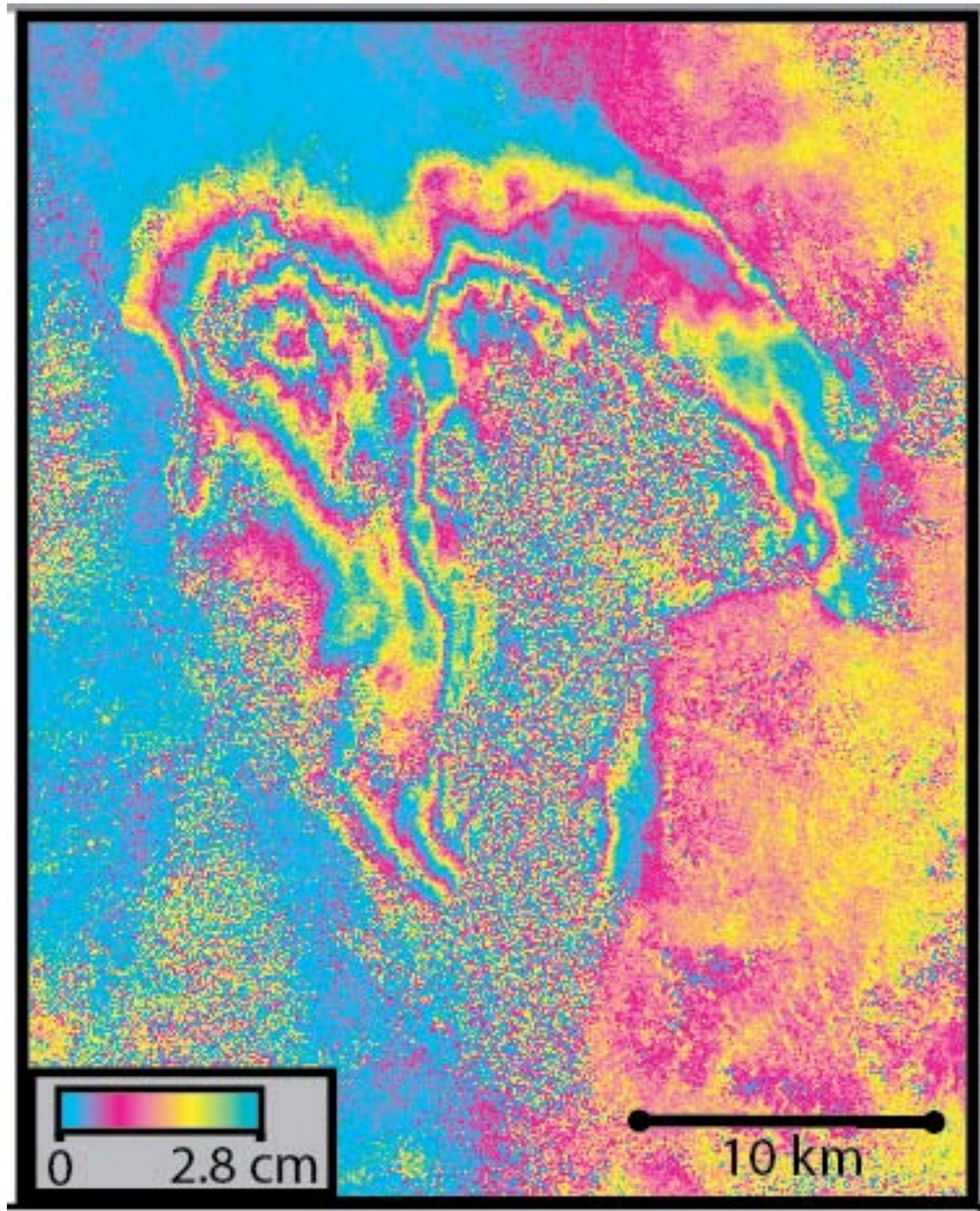
SUPPLEMENTAL FIGURE 2. Unwrapped interferogram of the Coso geothermal field spanning 3 Dec. 2009- 24 Nov. 2005 with cGPS stations labeled. Location shown on inset in Figure 1.



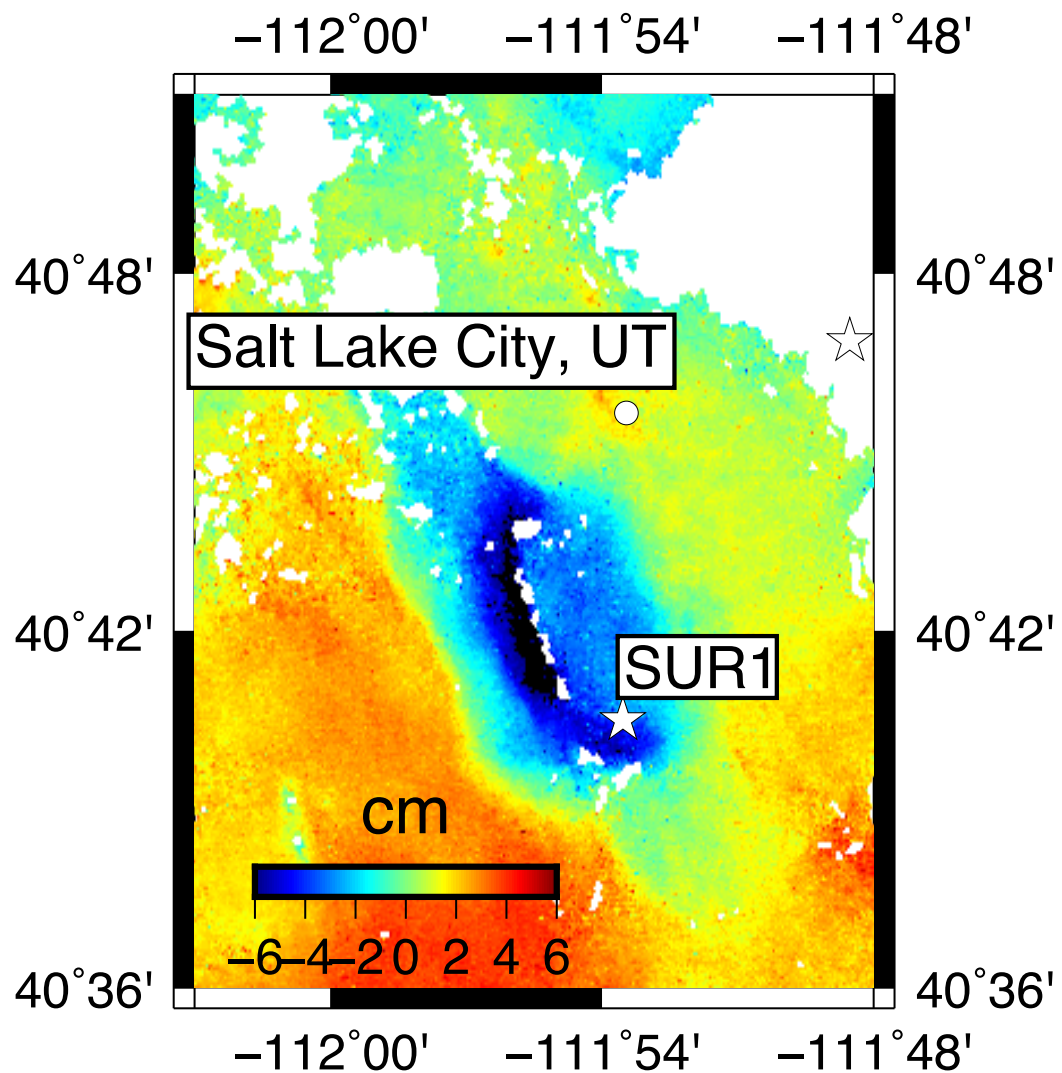
SUPPLEMENTAL FIGURE 3. Unwrapped interferogram covering Las Vegas from Envisat spanning 1 Feb. 2008 - 3 Sept. 2010 with cGPS stations labeled. Location shown on inset in Figure 1.



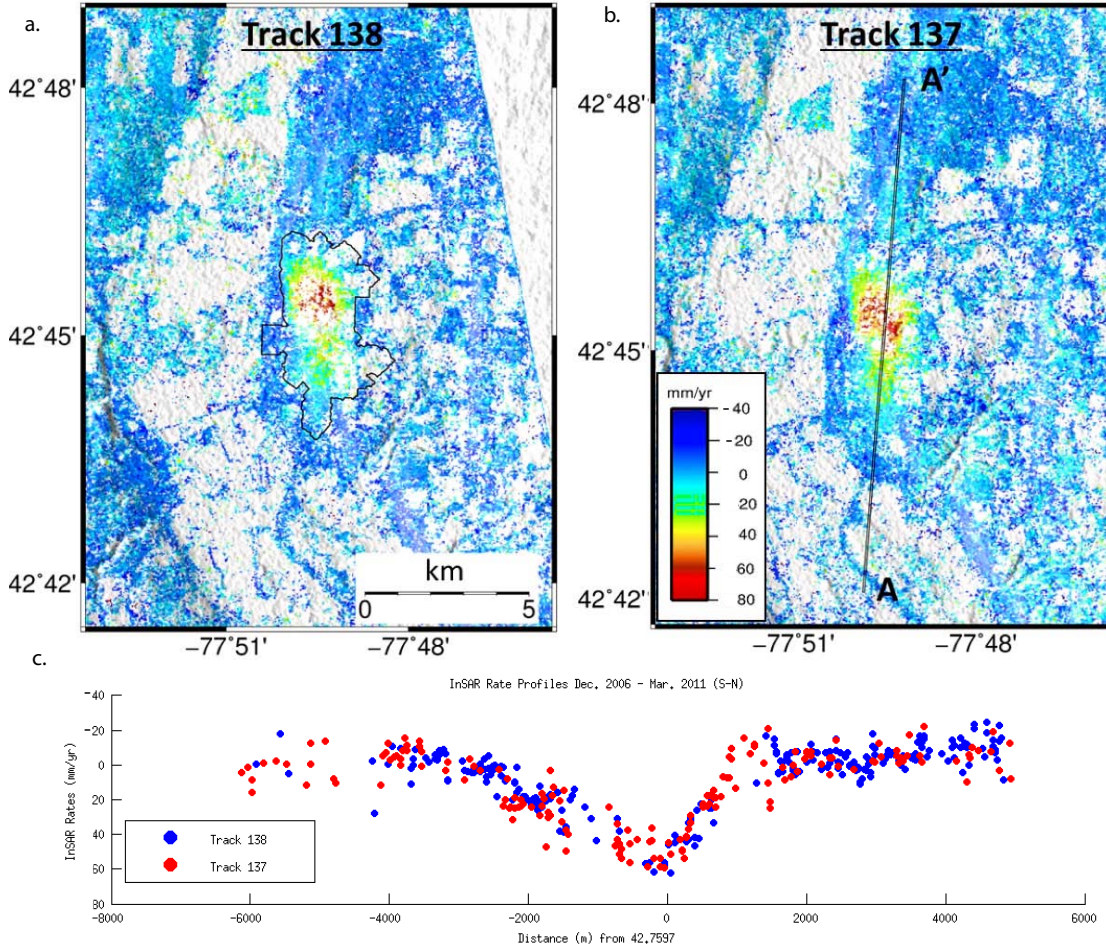
SUPPLEMENTAL FIGURE 4. Unwrapped interferogram covering East Mesa from Envisat spanning 1 Feb. 2008 - 3 Sept. 2010. Location shown on inset in Figure 1.



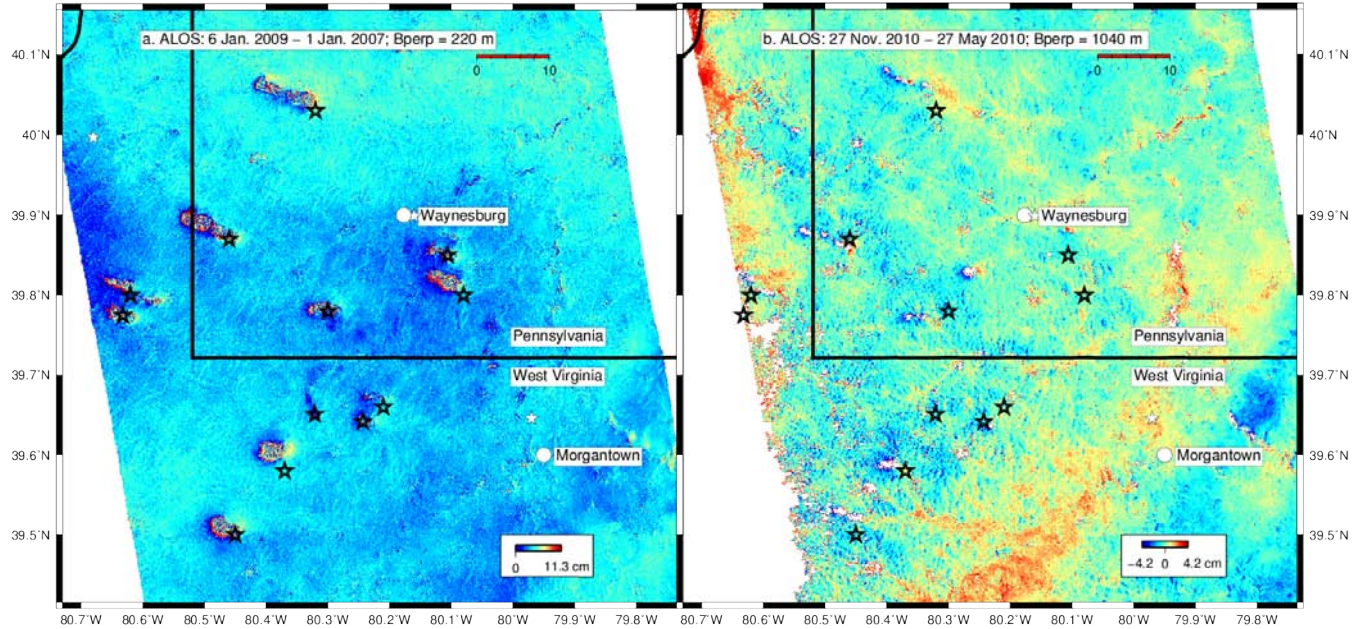
SUPPLEMENTAL FIGURE 5. Wrapped Envisat interferogram from 15 Oct. 2006-14 Sept. 2008 showing groundwater pumping subsidence in the Escalante Valley, Utah related to agriculture (*Forster, 2006*).



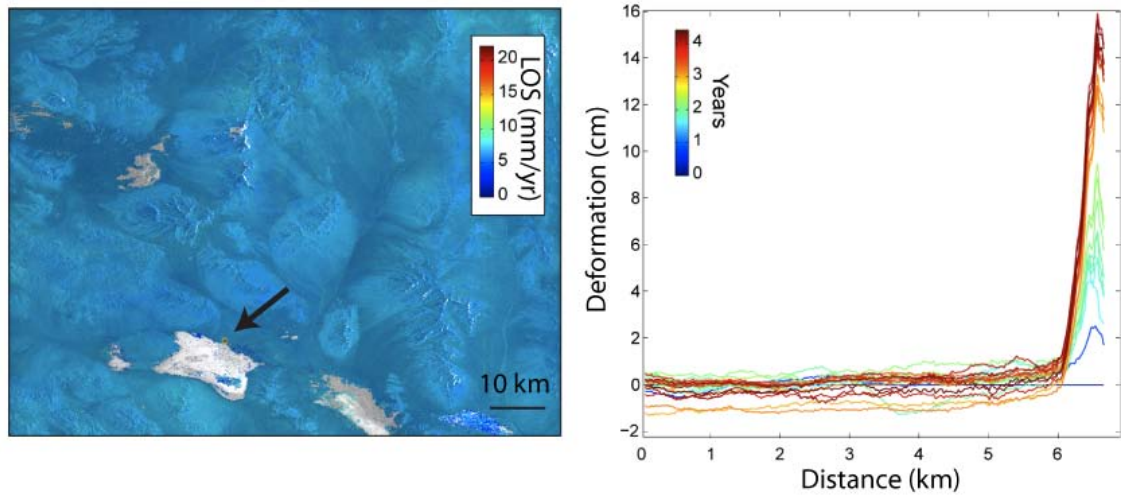
SUPPLEMENTAL FIGURE 6. Unwrapped interferogram from Envisat spanning 23 July 2009 to 18 February 2010 over Salt Lake City, UT showing that GPS station SUR1 is affected by the ground deformation. Stars indicate location of GPS sites.



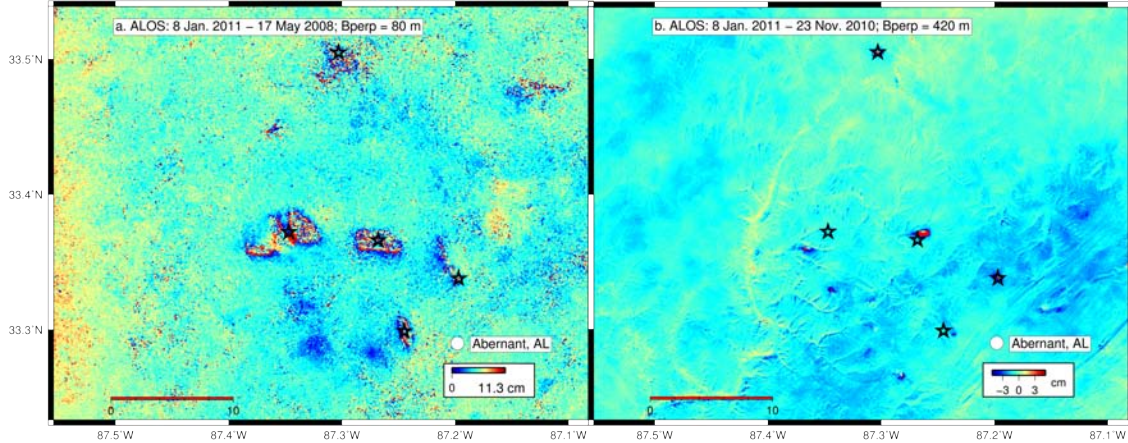
SUPPLEMENTAL FIGURE 7. a. and b. Time series from two paths of ALOS-1 data showing subsidence between 2006-2011 in western NY above a salt mine (outline from 2011 shown) (Valentino, 2016). The number of interferograms in paths 137 and 138 are 17 and 10, respectively. c. Profiles of the ALOS-1 time series from a. and b. (location of profile shown in b.). The maximum subsidence rate was about 8 cm/year and the RMS of pixels in the areas assumed to be non-deforming is 1.6 cm/yr, which is the approximate error on the rate.



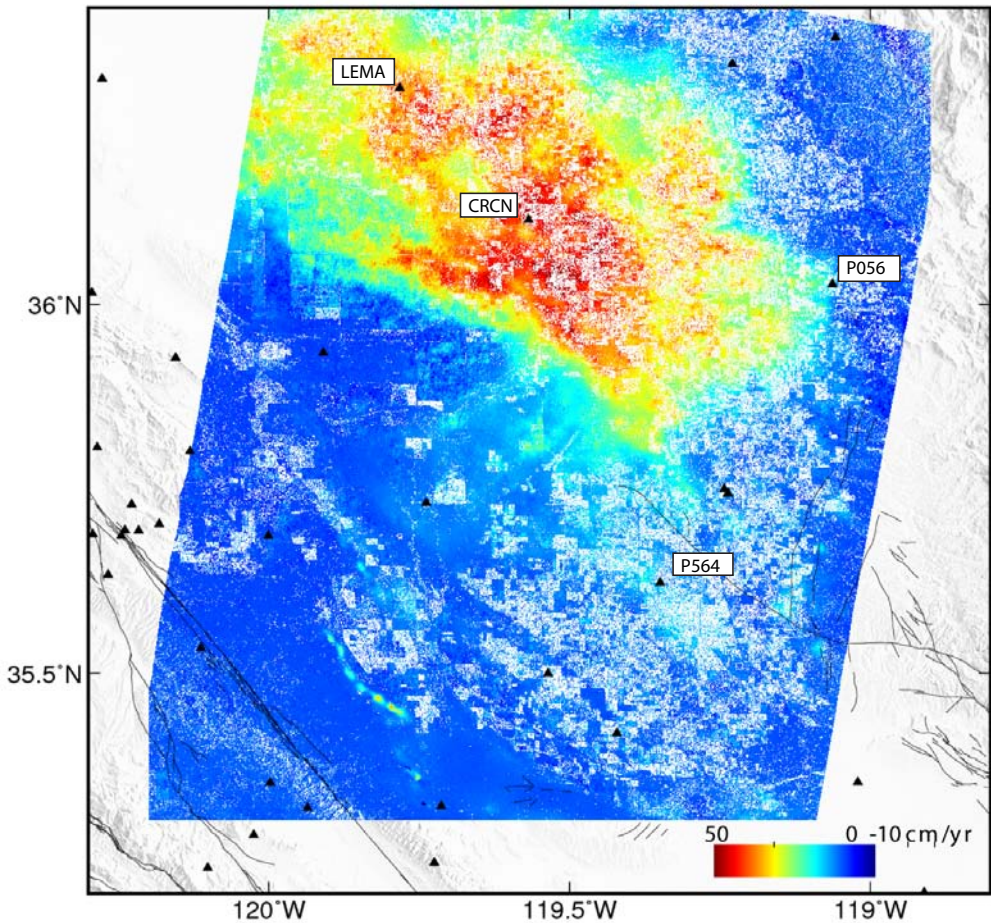
SUPPLEMENTAL FIGURE 8. ALOS interferograms spanning two years (left, 2007-2009) and six months (right, in 2010) over southwestern PA and northern WV showing ground deformation and decorrelated areas suspected to be related to underground coal mines (inferred locations shown as black stars). We do not think the phase changes or decorrelation are due to topographic errors in the DEM because the shorter interferogram with the larger perpendicular baseline (right, that is more sensitive to topographic change) does not show the effects seen in the longer time period interferogram with the shorter perpendicular baseline. The interferogram on the left was made using the 10 m/pixel NED DEM while the interferogram on the right was made using the 30 m/pixel SRTM DEM because the interferogram was noisier with the NED DEM. Locations of publically available continuous GPS observations are shown as white stars – none appear contaminated by the deformation.



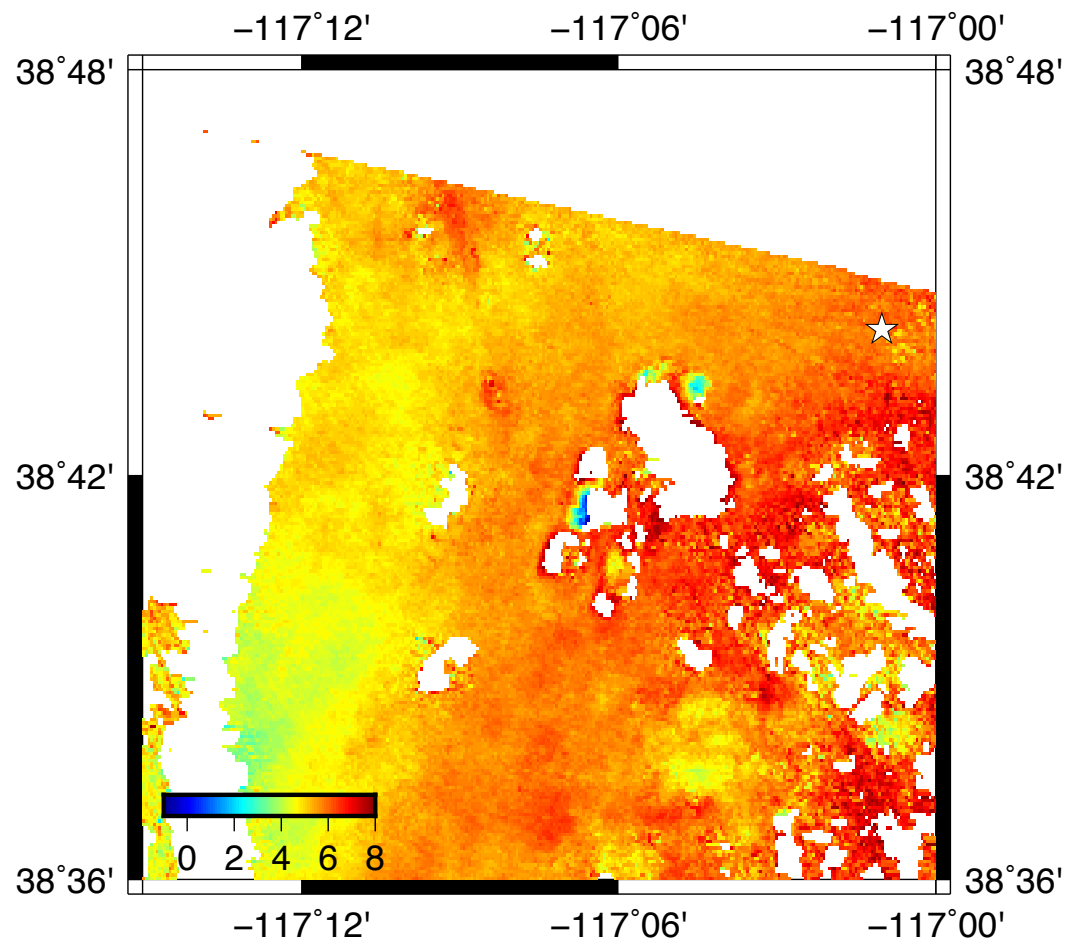
SUPPLEMENTAL FIGURE 9. InSAR time series (Envisat) for Track 356/Frame 2907, showing high subsidence rate ($> 2 \text{ cm/yr}$, left panel) associated with withdrawal of water at a salt evaporation facility near Amboy Crater, Southern California. Right panel shows the cumulative deformation as a function of date (colored by year), illustrating the steady subsidence at this site.



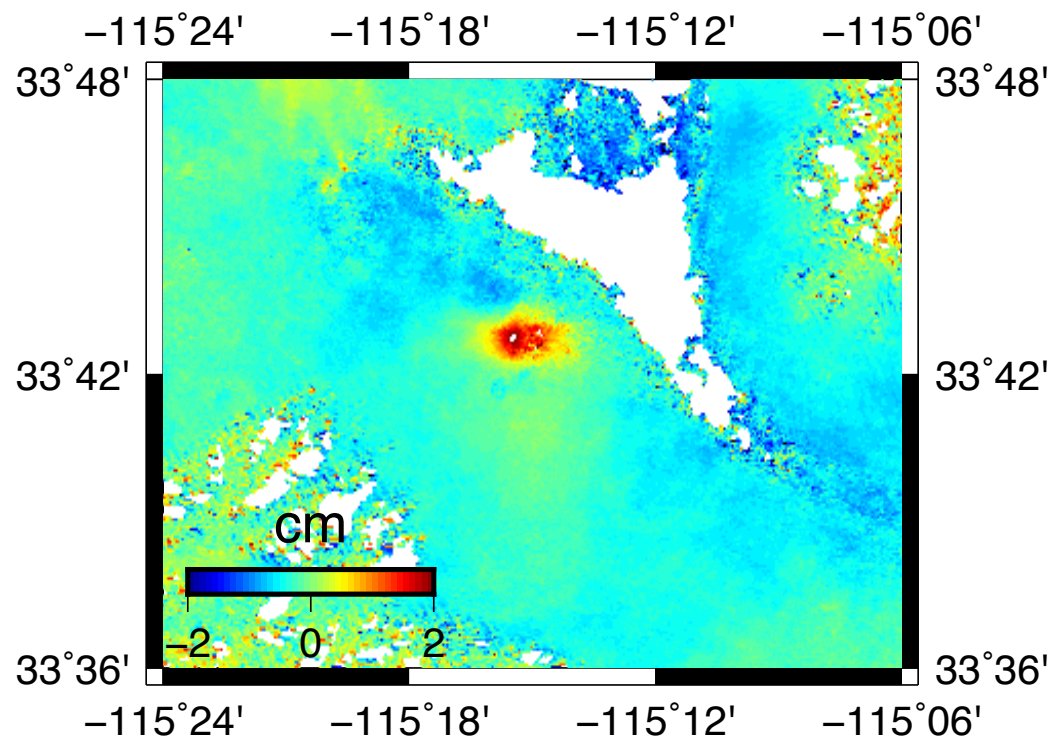
SUPPLEMENTAL FIGURE 10. ALOS interferograms spanning two years (left, 2008-2011) and 46 days (right, in 2010-2011) over Tuscaloosa County, Alabama showing ground deformation and decorrelated areas suspected to be related to surface and underground coal mines (inferred locations shown as black stars). We do not think the phase changes or decorrelation are only due to topographic errors in the DEM because the shorter interferogram with the larger perpendicular baseline (right, that is more sensitive to topographic change) does not show the effects seen in the longer time period interferogram with the shorter perpendicular baseline (left panel). Both images used the 30/pixel NED DEM. There are no GPS observations in this area.



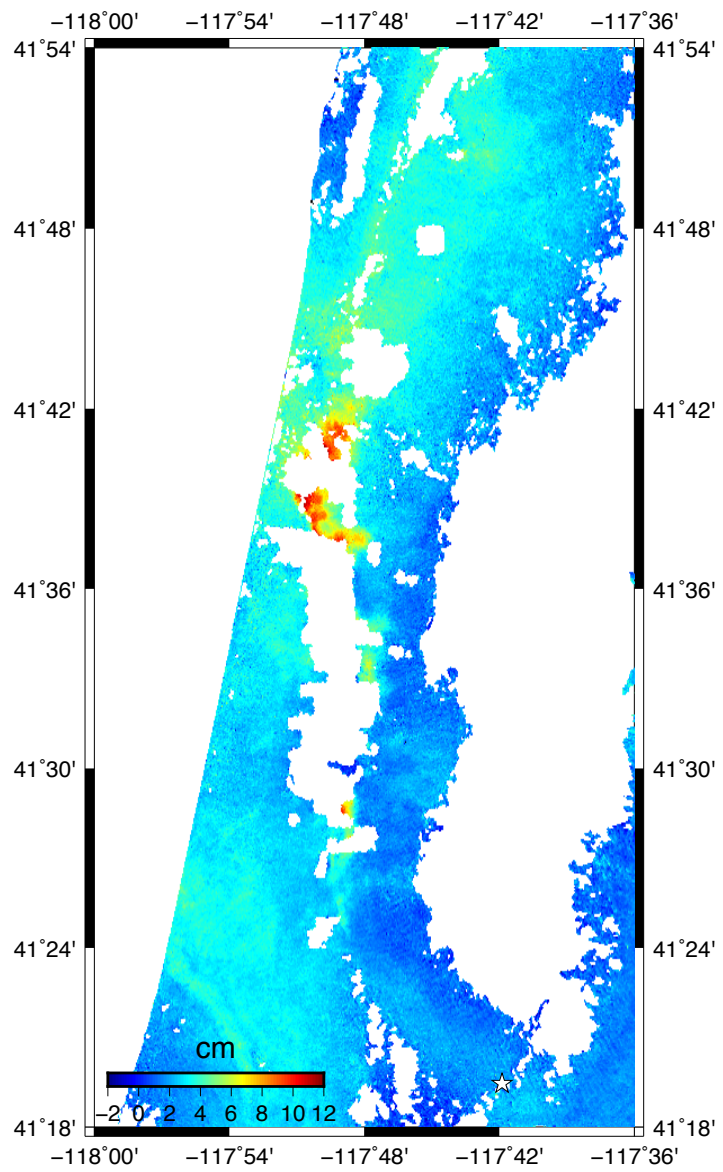
SUPPLEMENTAL FIGURE 11. Time series of deformation from the Central Valley of California from the Sentinel-1a/b platforms (ESA) spanning October, 2014 - August, 2017 processed by Kyle D. Murray. Black triangles show locations of continuous GPS data archived at UNAVCO, with a few additional sites from the compilation by the University of Nevada, Reno (<http://geodesy.unr.edu/NGLStationPages/gpsnetmap/GPSNetMap.html>). Sites of deformation are similar in the Envisat time series (not shown) between January 2008 - September 2010. Faults shown as line segments are from USGS and CGS (2006).



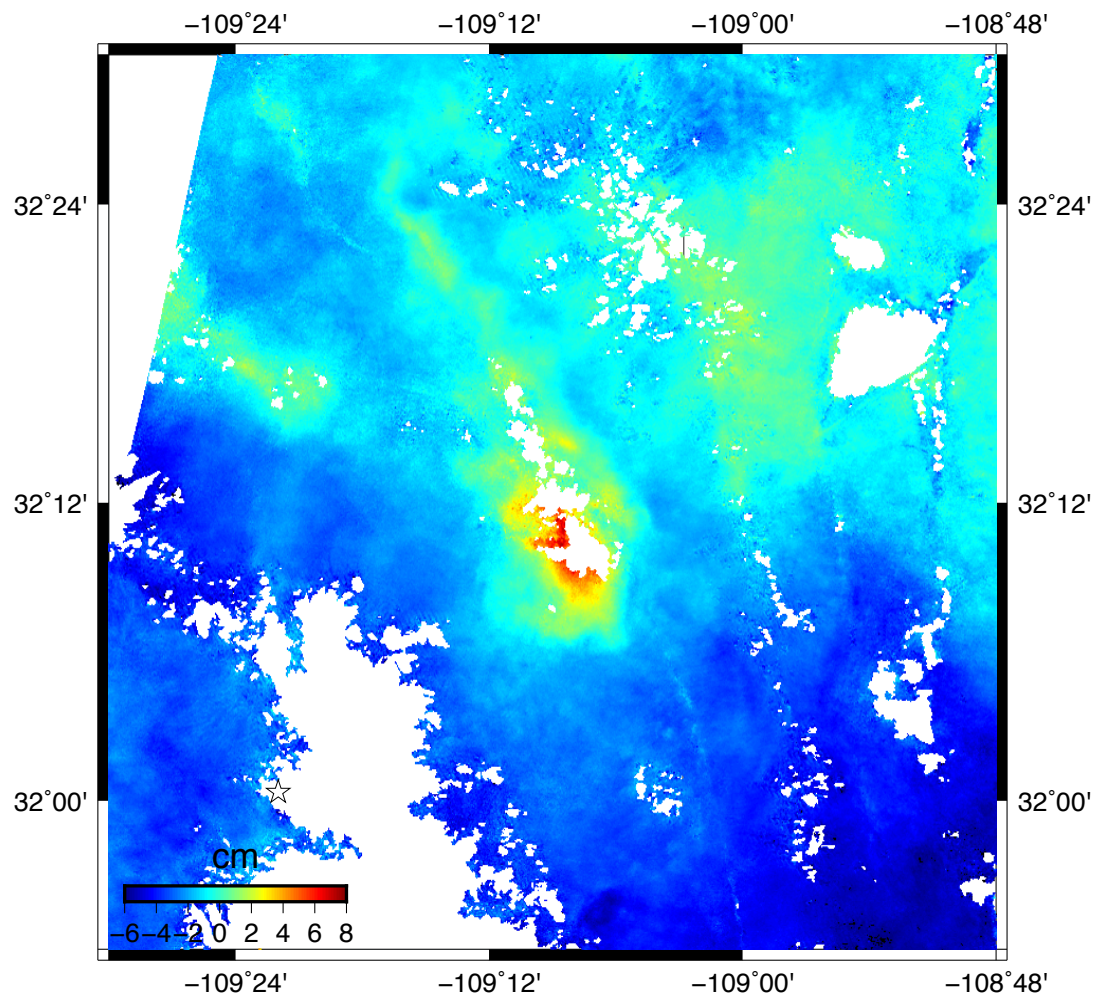
SUPPLEMENTAL FIGURE 12. Interferogram of Round Mountain Mine, NV from Envisat spanning 4 Sept. 2008- 26 June 2006. Stars indicate location of GPS sites.



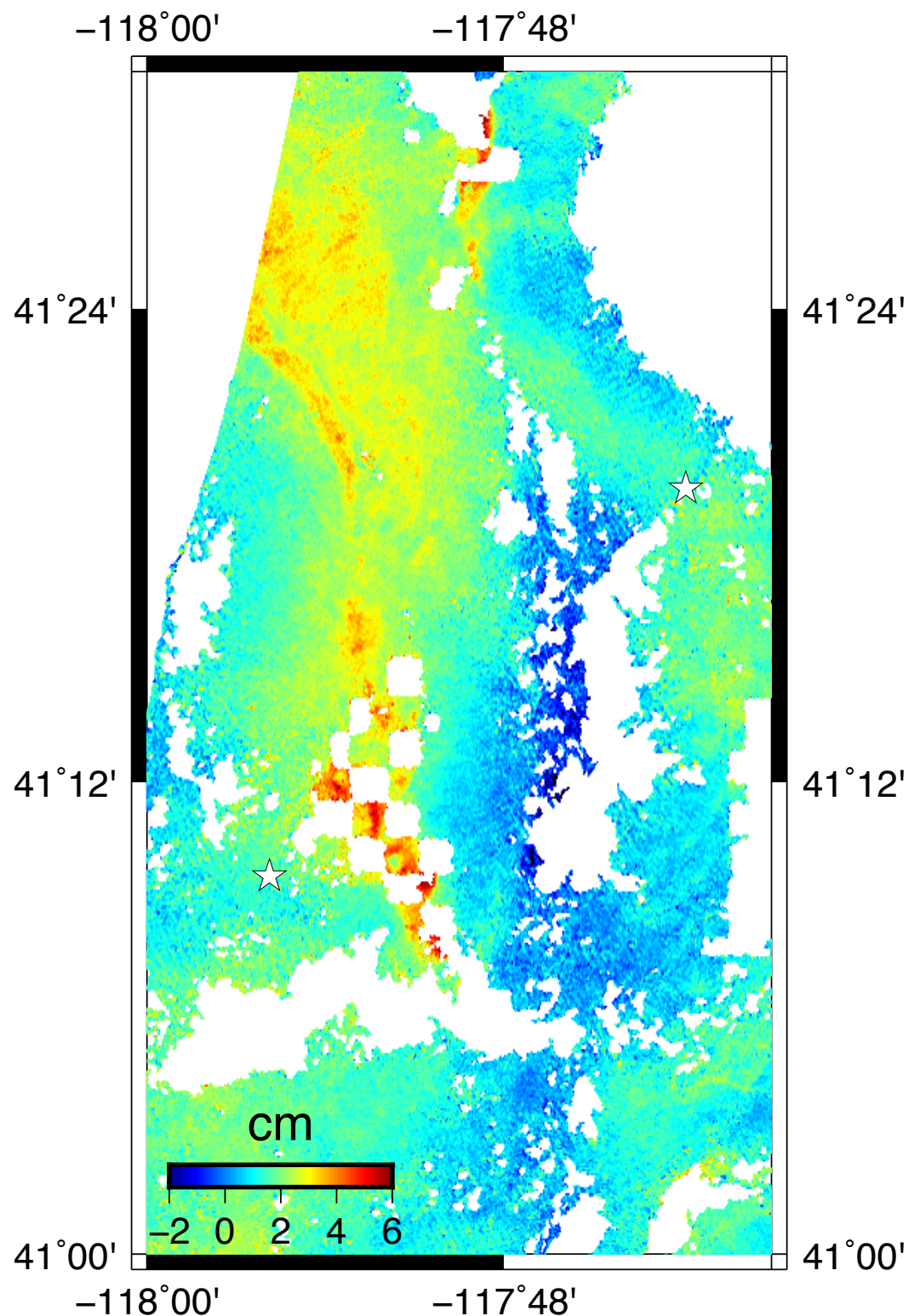
SUPPLEMENTAL FIGURE 13. Interferogram of Palm Tree Farm, CA from Envisat spanning 4 Nov. 2007 - 4 March 2007.



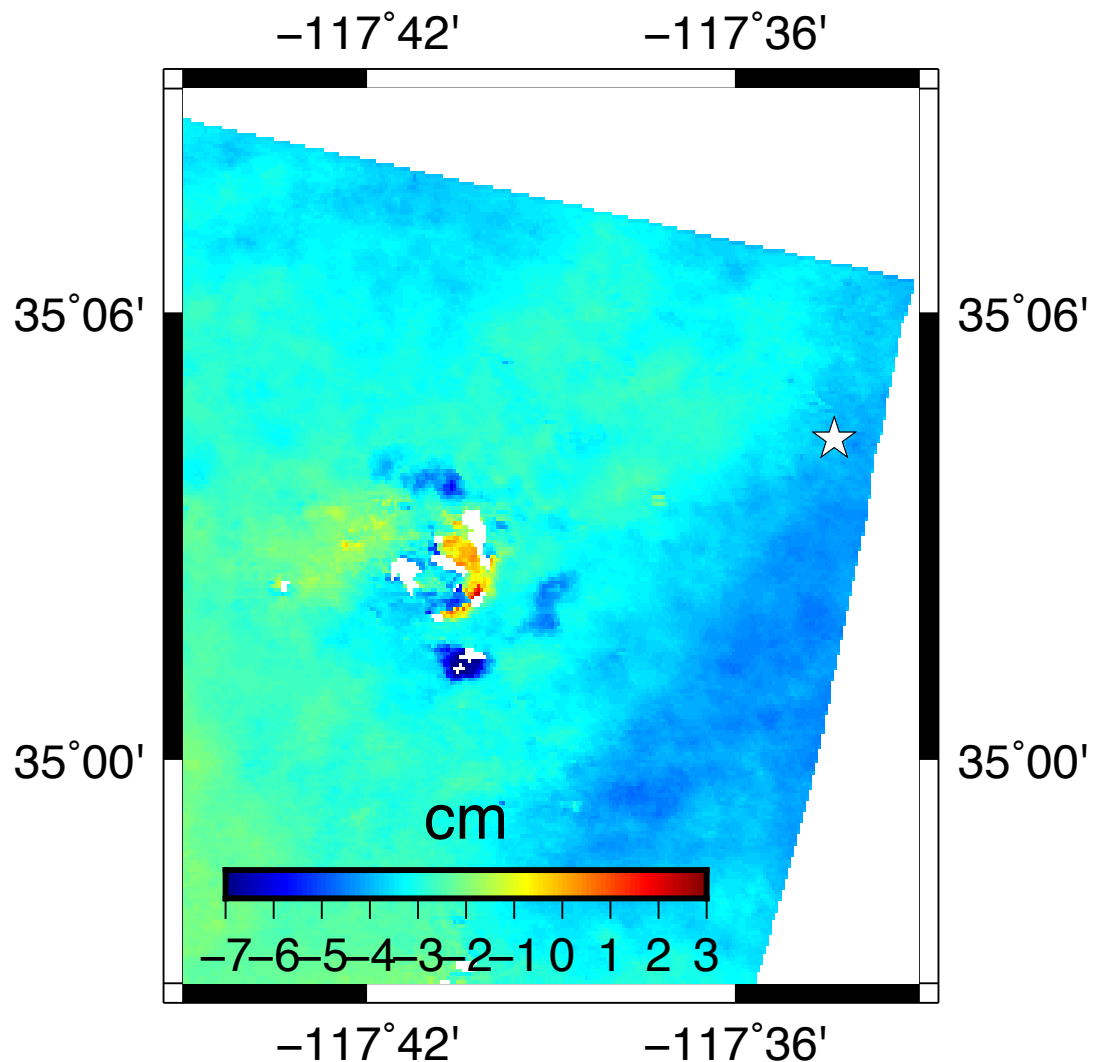
SUPPLEMENTAL FIGURE 14. Interferogram of Quinn River Valley, NV from Envisat spanning 23 Sept. 2008 - 26 June 2007.



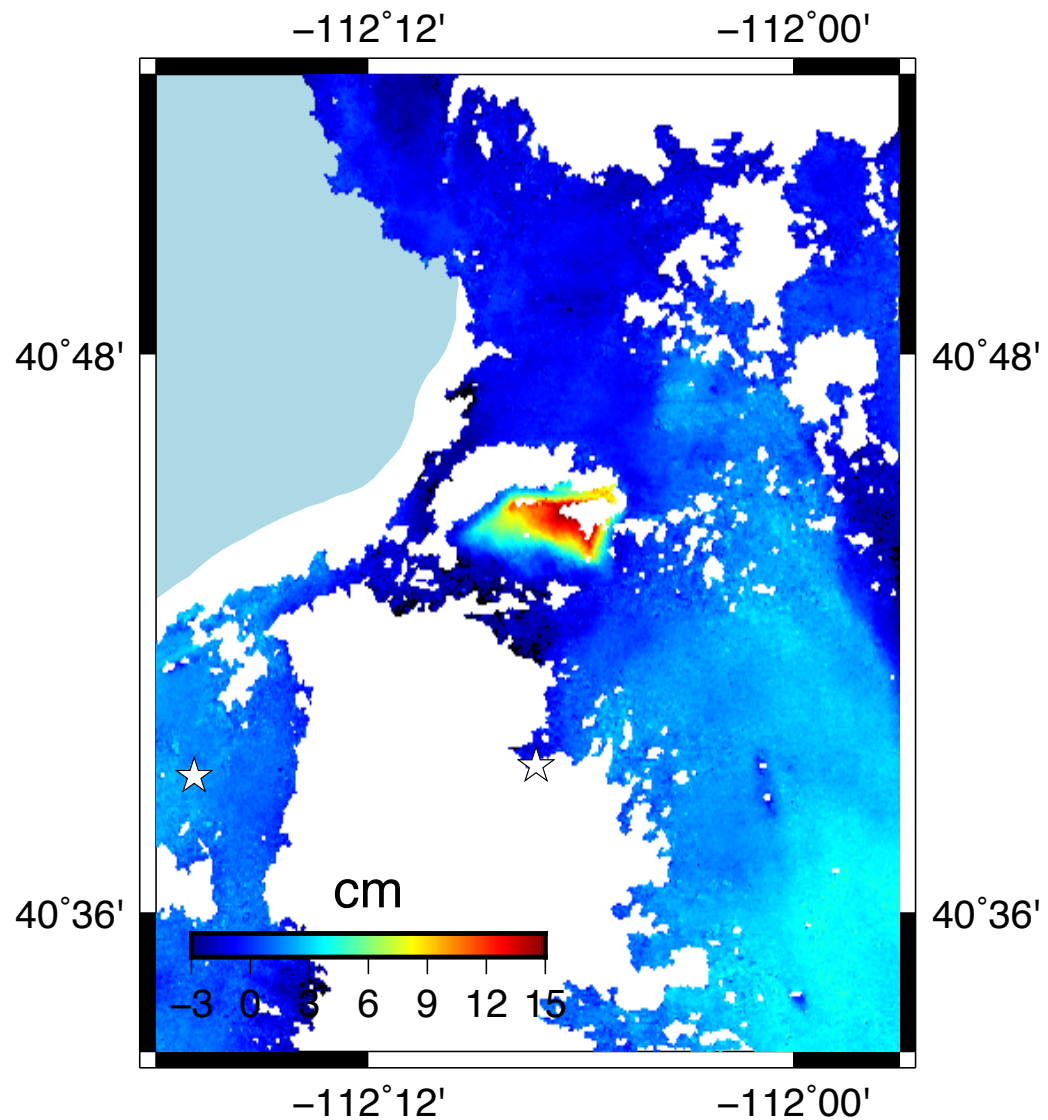
SUPPLEMENTAL FIGURE 15. Interferogram of San Simon, NM from Envisat spanning 15 July 2010 - 17 Dec. 2009. Stars indicate location of GPS sites.



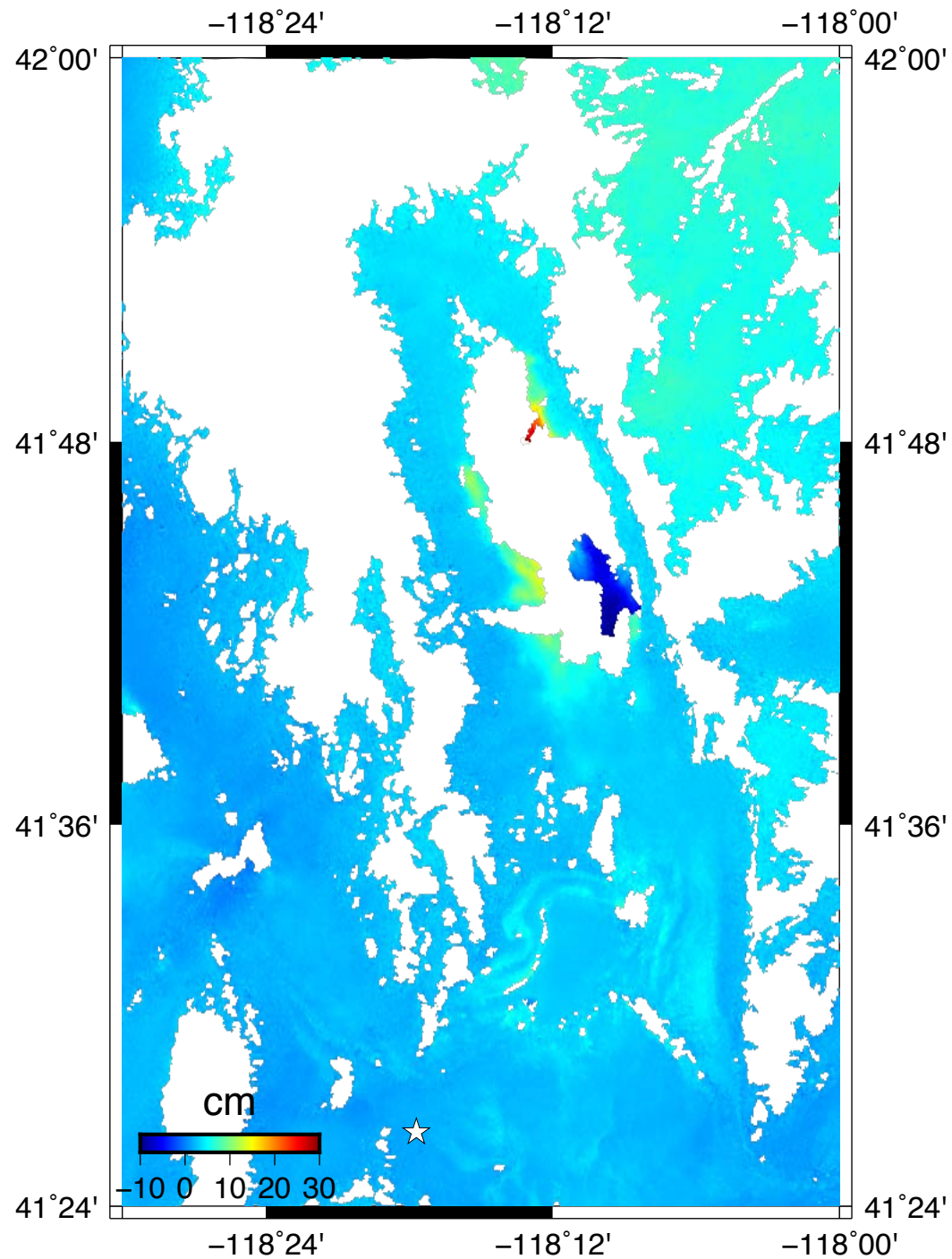
SUPPLEMENTAL FIGURE 16. Interferogram of Silver State Valley, NV from Envisat spanning 23 Sept. 2008 - 26 June 2007. Stars indicate location of GPS sites.



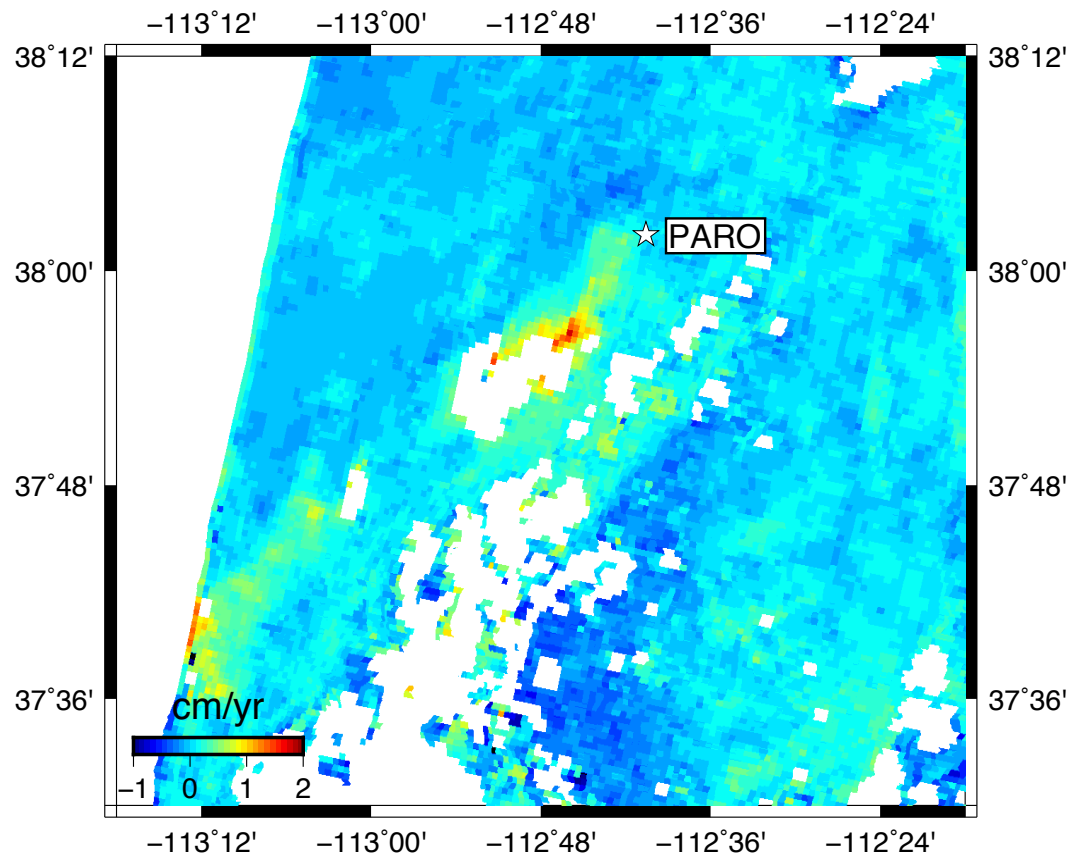
SUPPLEMENTAL FIGURE 17. Interferogram of US Borax Mine, CA from Envisat spanning 4 Sept. 2008 - 26 June 2008. Stars indicate location of GPS sites.



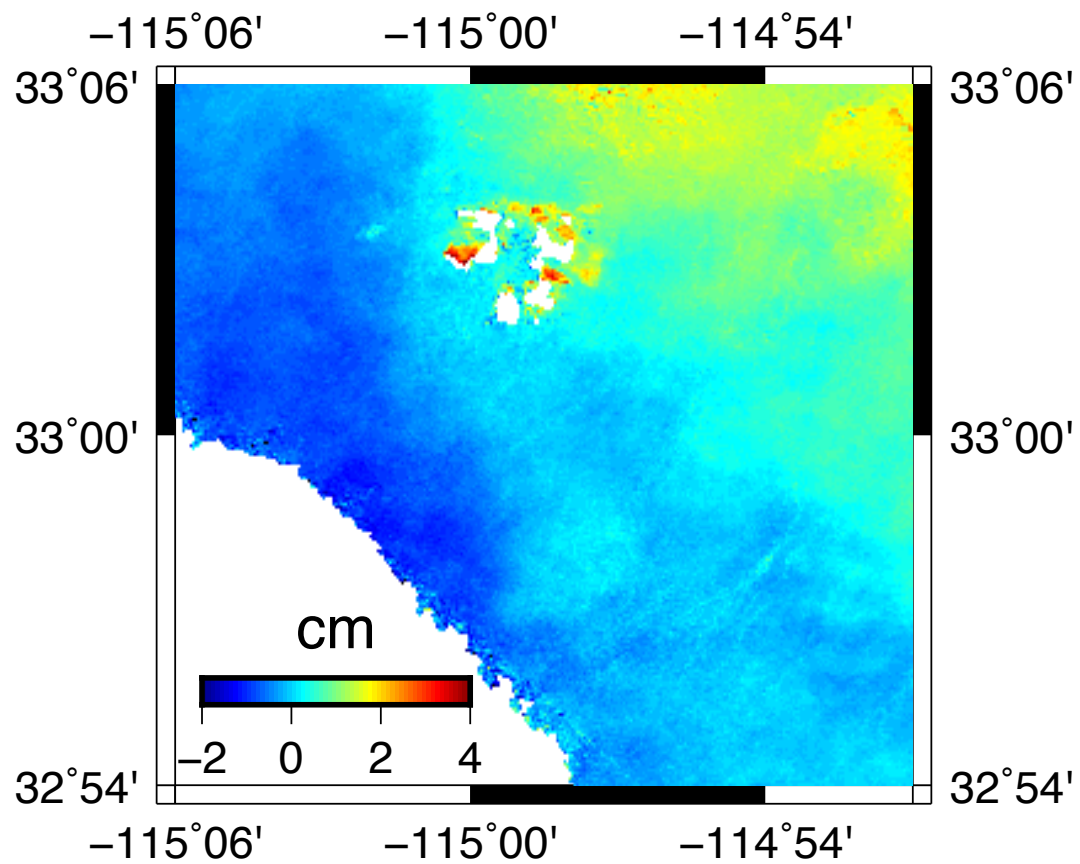
SUPPLEMENTAL FIGURE 18. Interferogram of Kennecott, UT from Envisat spanning 18 Feb. 2010 - 23 July 2009. Stars indicate location of GPS sites.



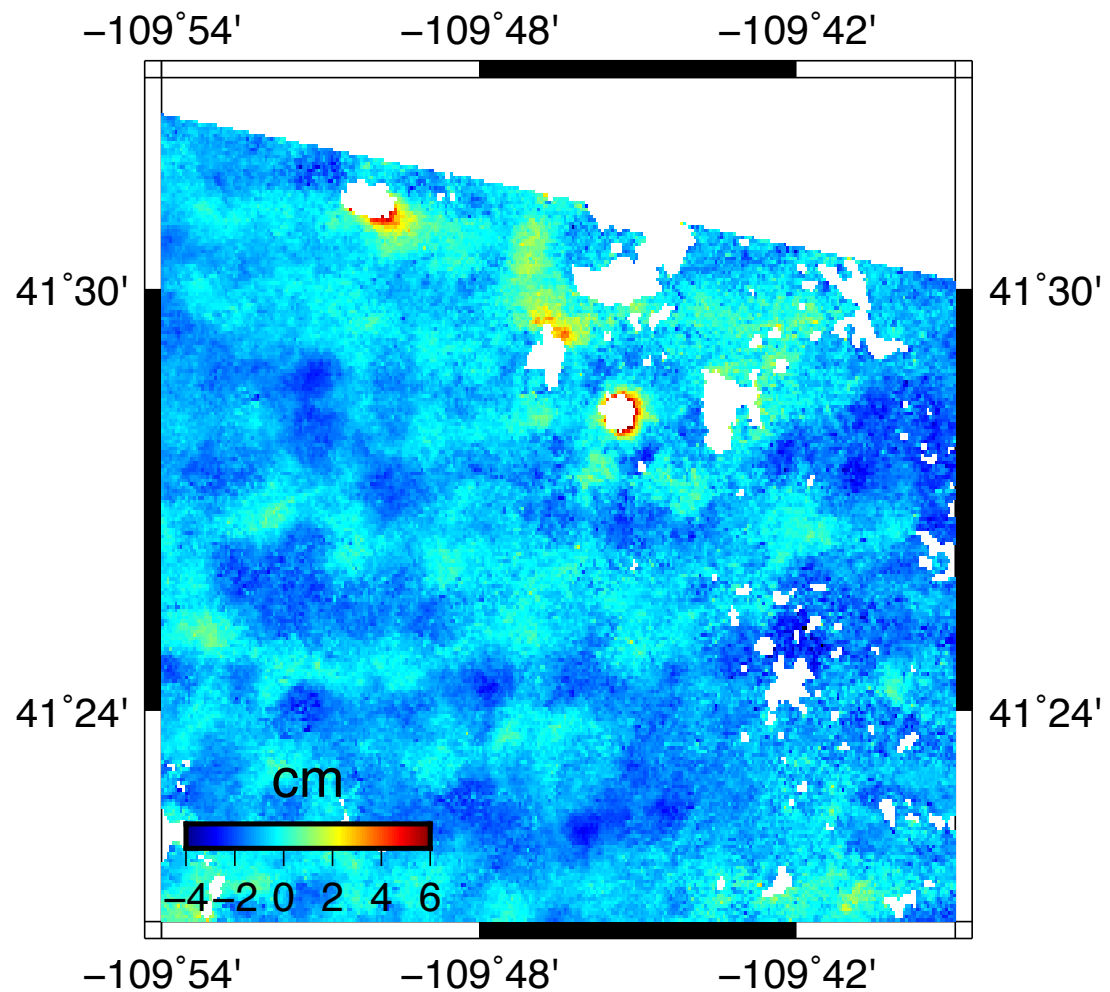
SUPPLEMENTAL FIGURE 19. Interferogram of Kings River Valley, NV from Envisat spanning 1 Oct. 2010 - 22 Aug. 2008.



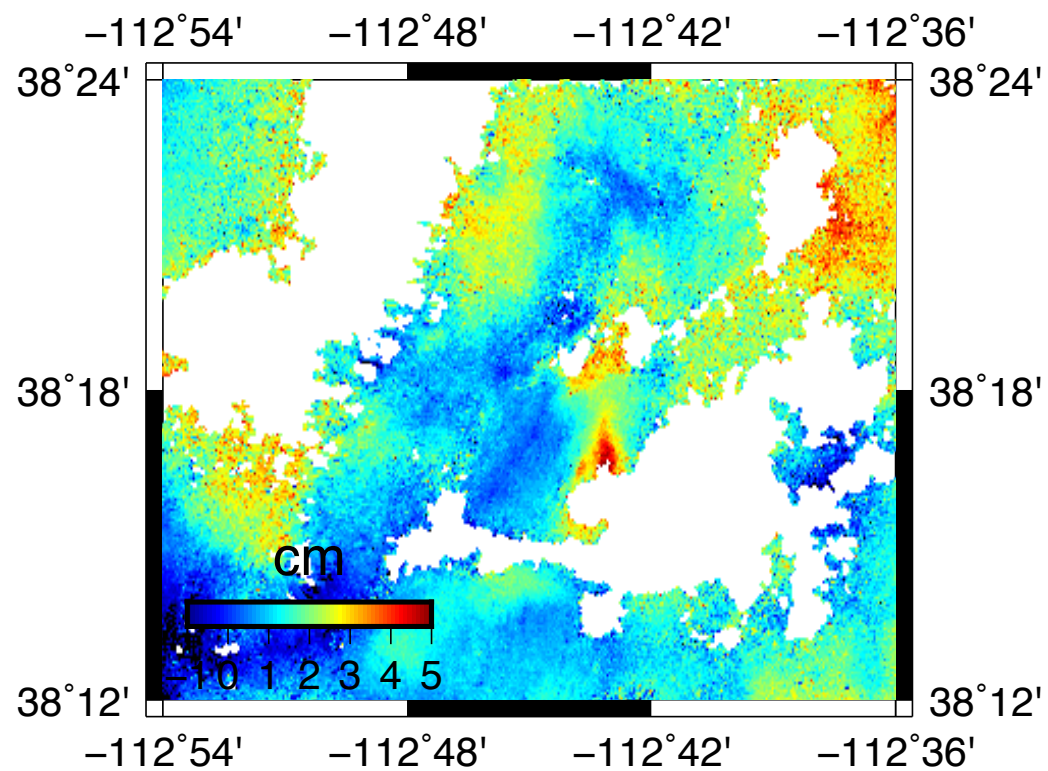
SUPPLEMENTAL FIGURE 20. Time series of Little Salt Lake, UT from Envisat spanning 16 Sept. 2010 - 5 Nov. 2009. Stars indicate location of GPS sites – site PARO is potentially affected.



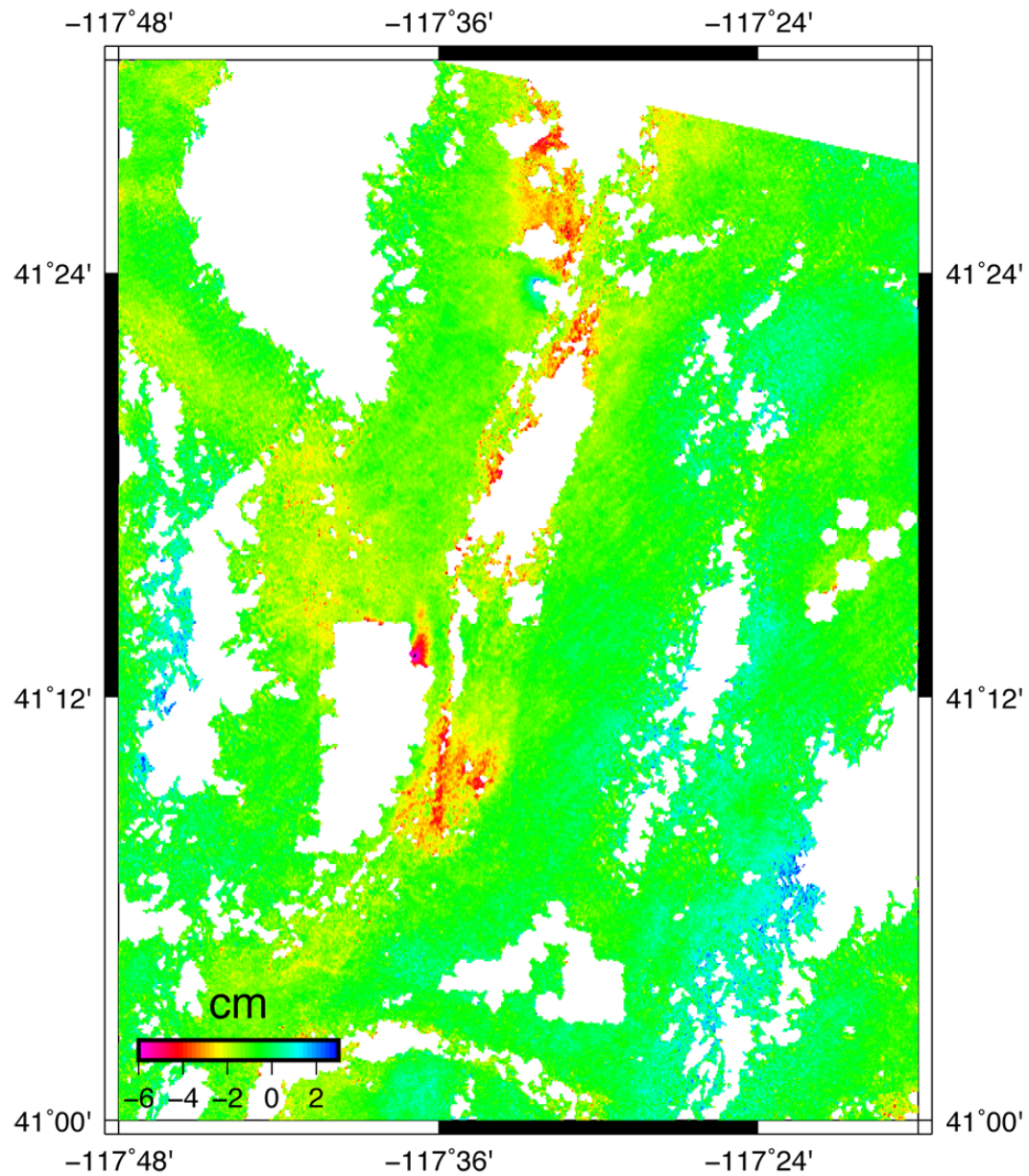
SUPPLEMENTAL FIGURE 21. Interferogram of Mesquite Mine, CA from Envisat spanning 4 Nov. 2007 - 19 March 2006.



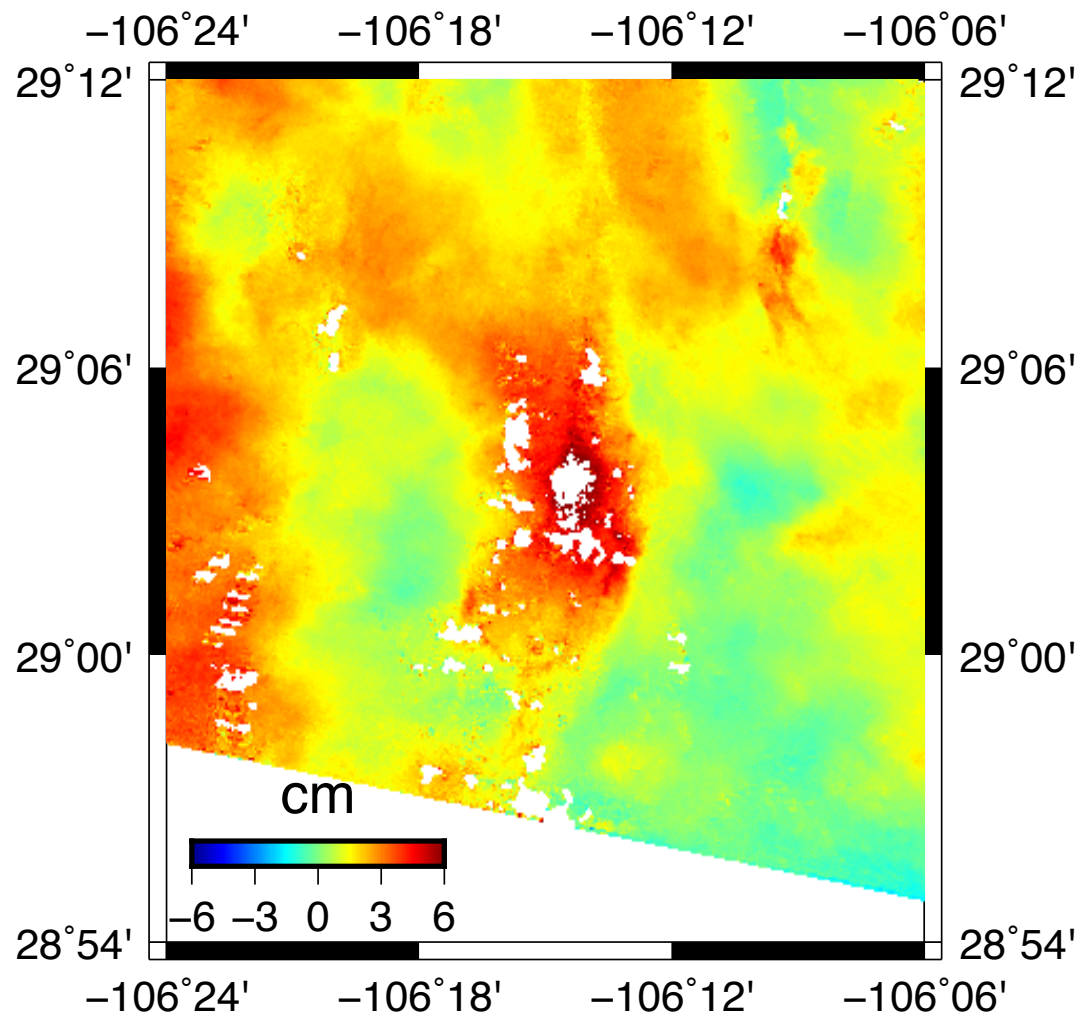
SUPPLEMENTAL FIGURE 22. Interferogram of Little America, WY from Envisat spanning 9 Sept. 2009 - 27 May 2009.



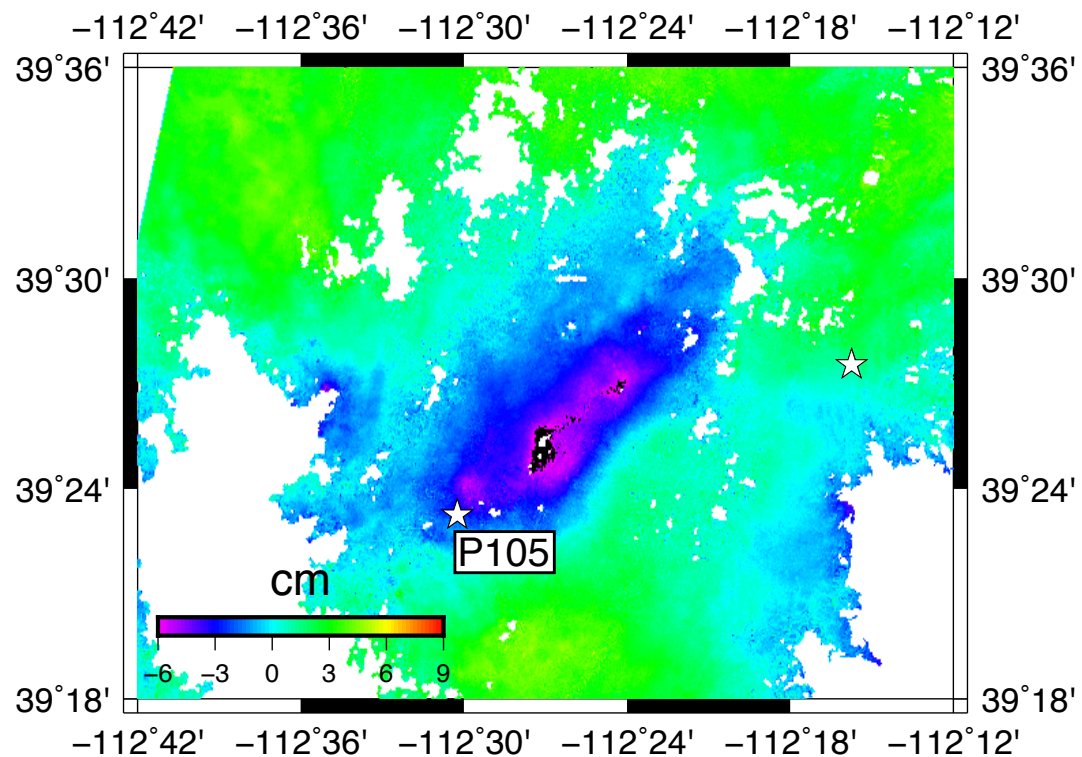
SUPPLEMENTAL FIGURE 23. Interferogram near Beaver, UT from Envisat spanning 12 Aug. 2010 - 9 April 2009.



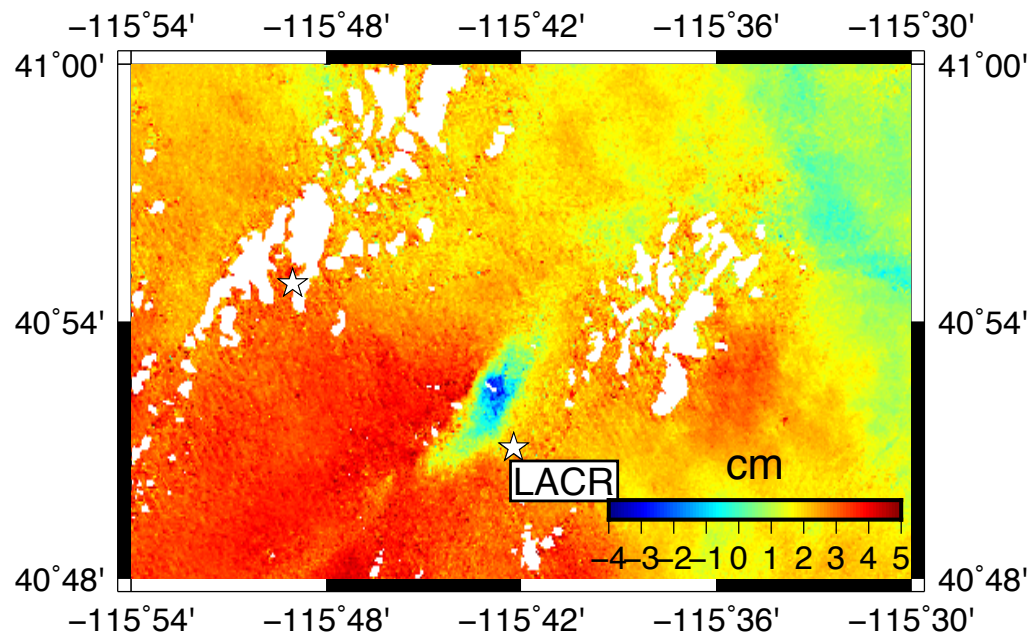
SUPPLEMENTAL FIGURE 24. Interferogram of North and South Paradise Valley, NV from Envisat spanning 23 Sept. 2008 - 26 June 2007.



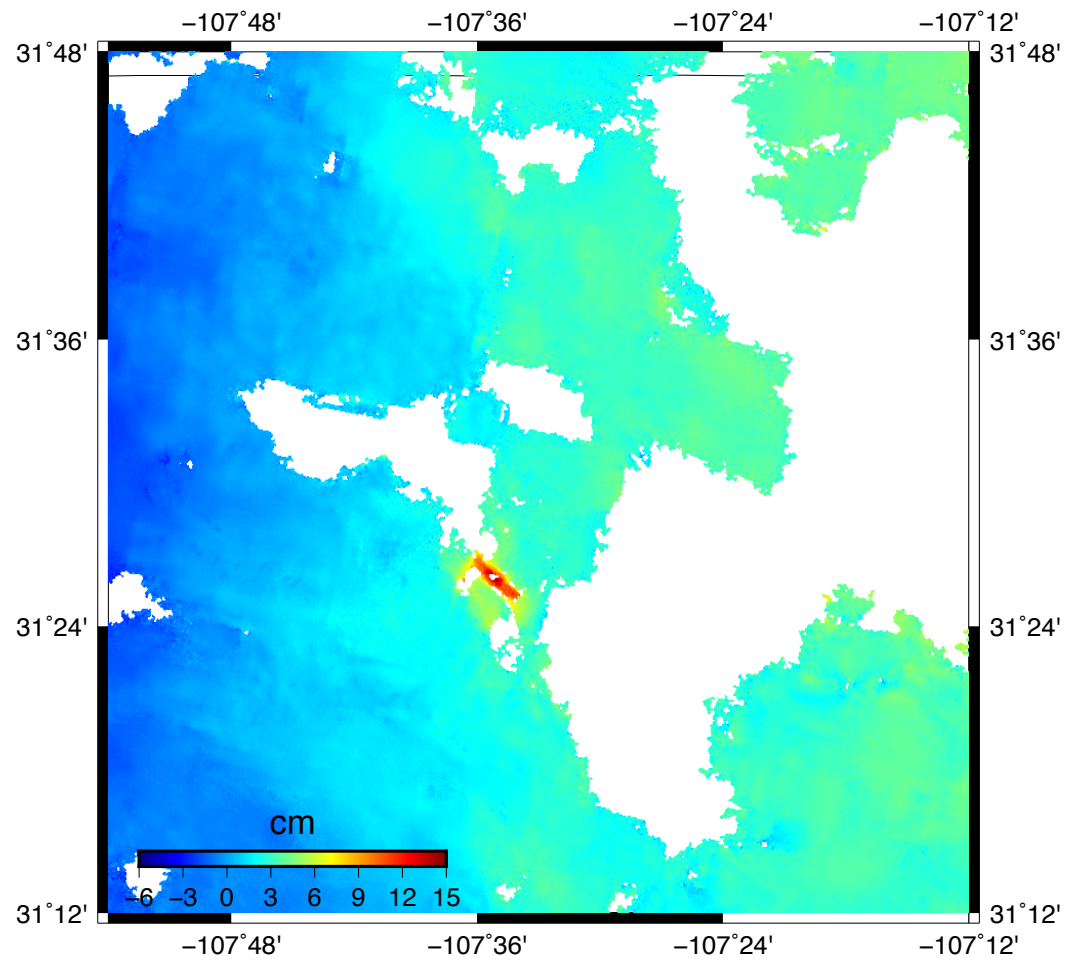
SUPPLEMENTAL FIGURE 25. Interferogram of Nuevo Delicias, Mexico from ERS spanning 13 April 1996 - 30 Dec. 1995.



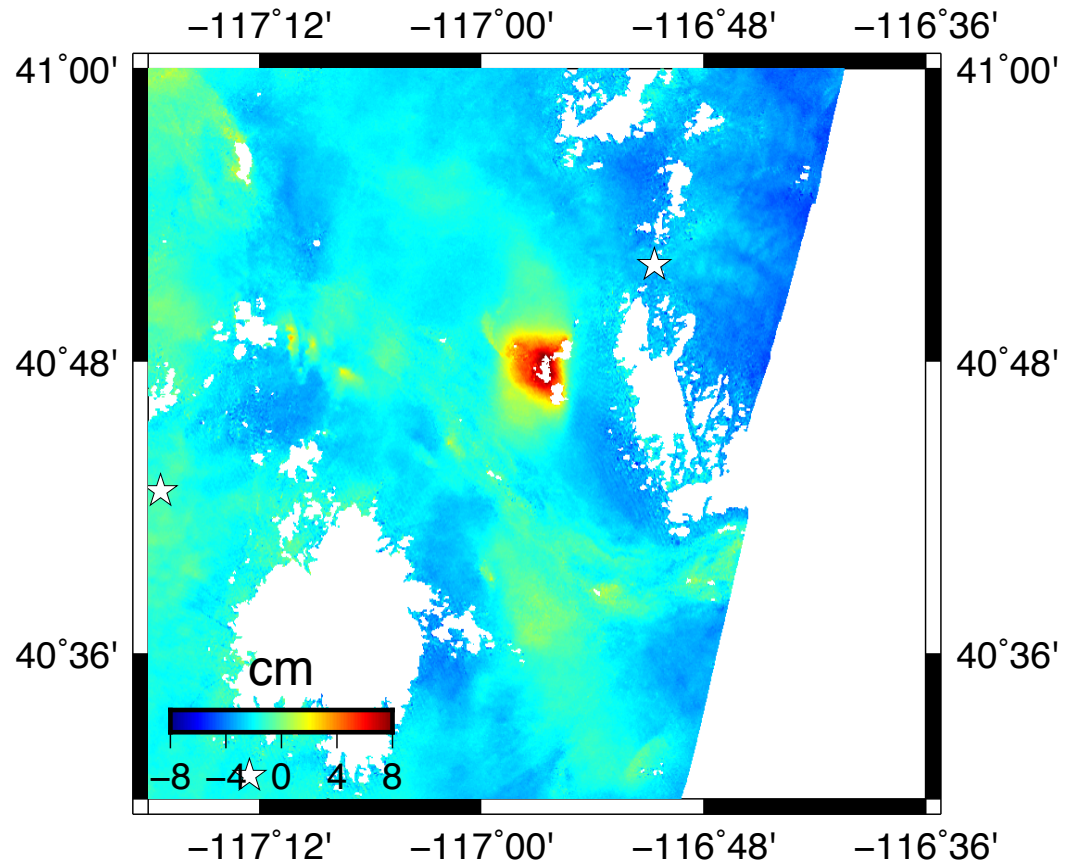
SUPPLEMENTAL FIGURE 26. Interferogram of DMAD Reservoir, UT from Envisat spanning 18 Feb. 2010 - 23 July 2009. Stars indicate location of GPS sites – site P105 is affected.



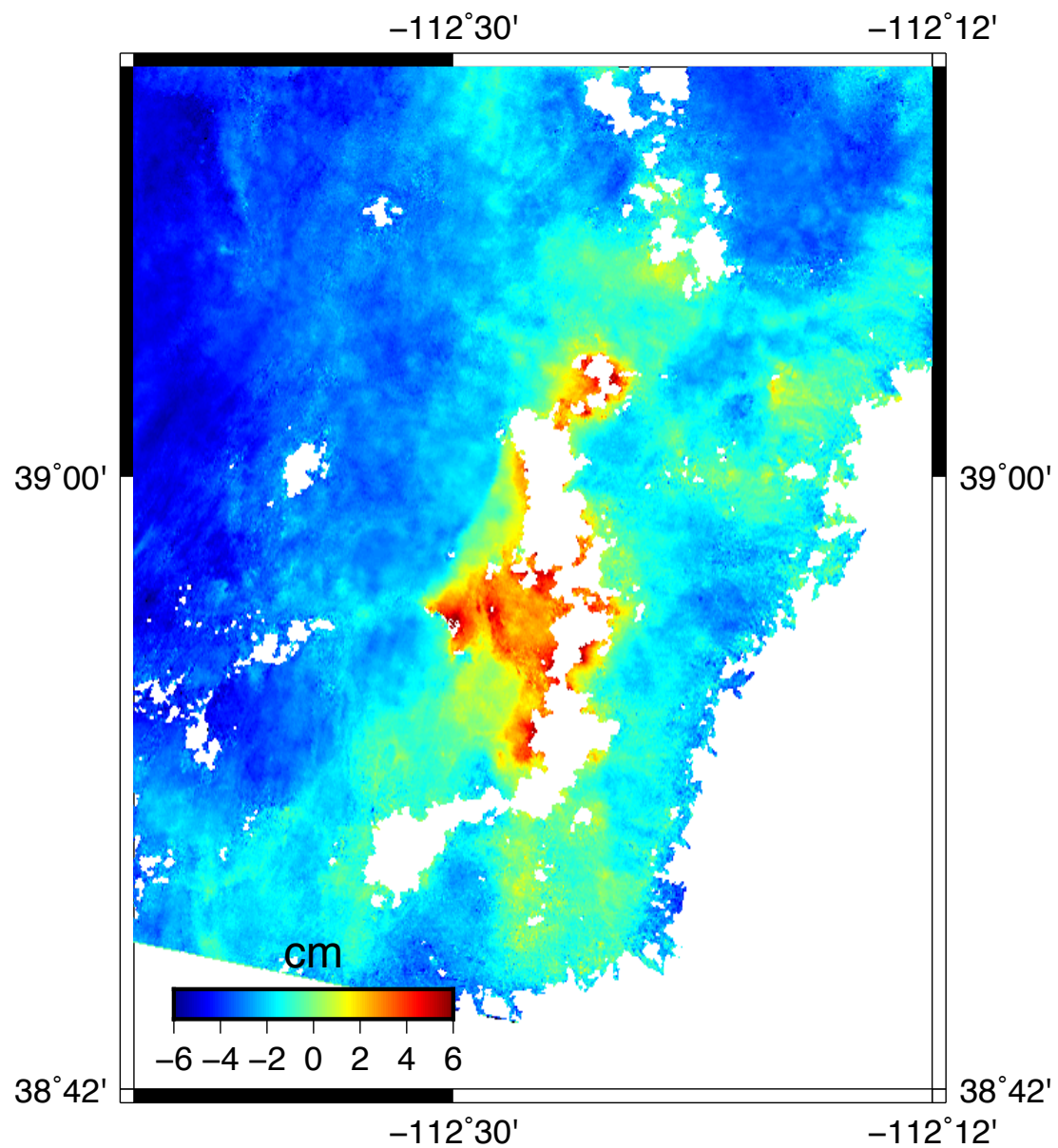
SUPPLEMENTAL FIGURE 27. Interferogram of Elko, NV from Envisat spanning 26 Nov. 2007 - 17 Sept. 2007. Stars indicate location of GPS sites – site LACR could be affected.



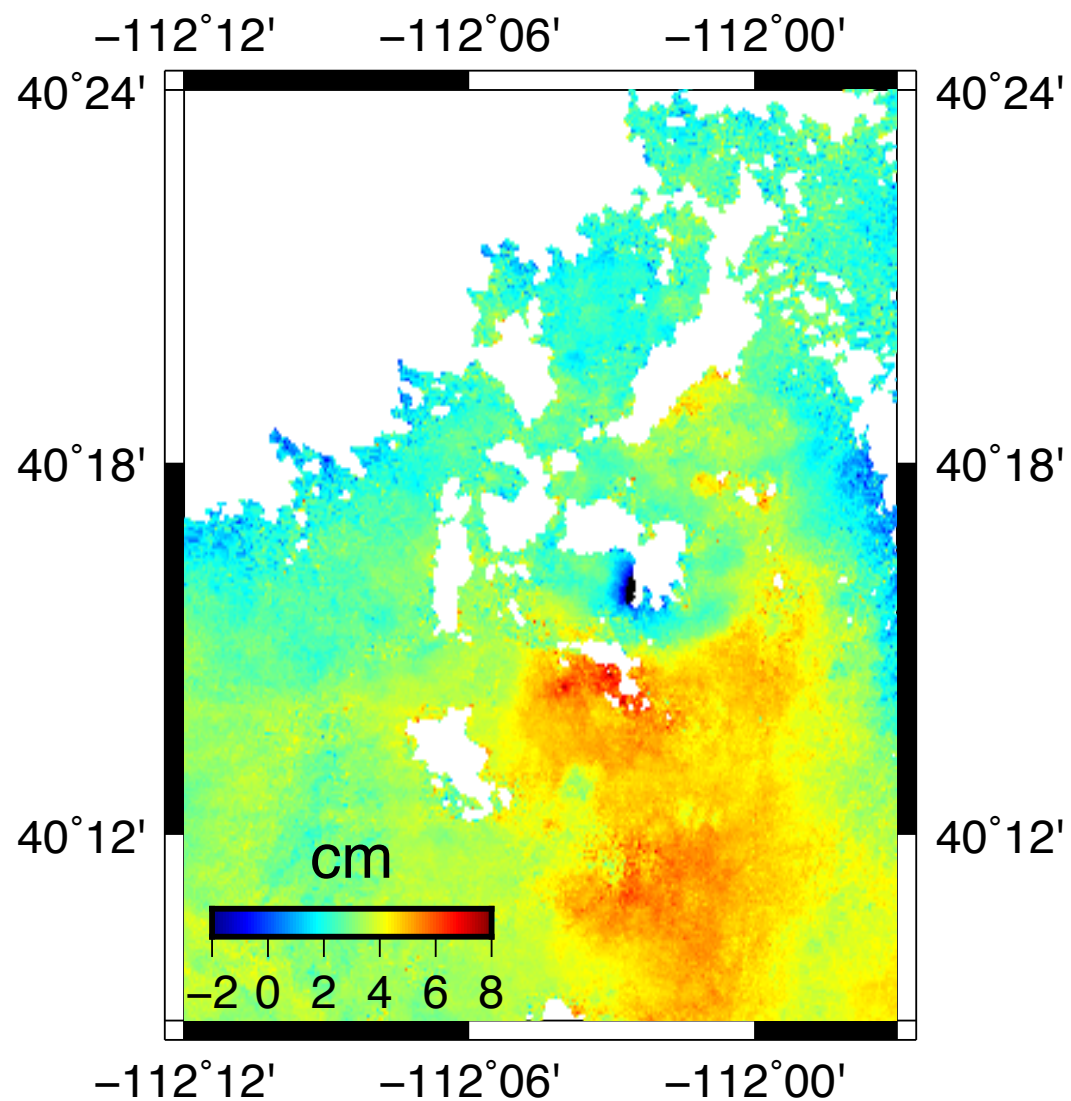
SUPPLEMENTAL FIGURE 28. Interferogram of E Los Trios, Mexico from Envisat spanning 7 June 2010 - 5 Nov. 2007.



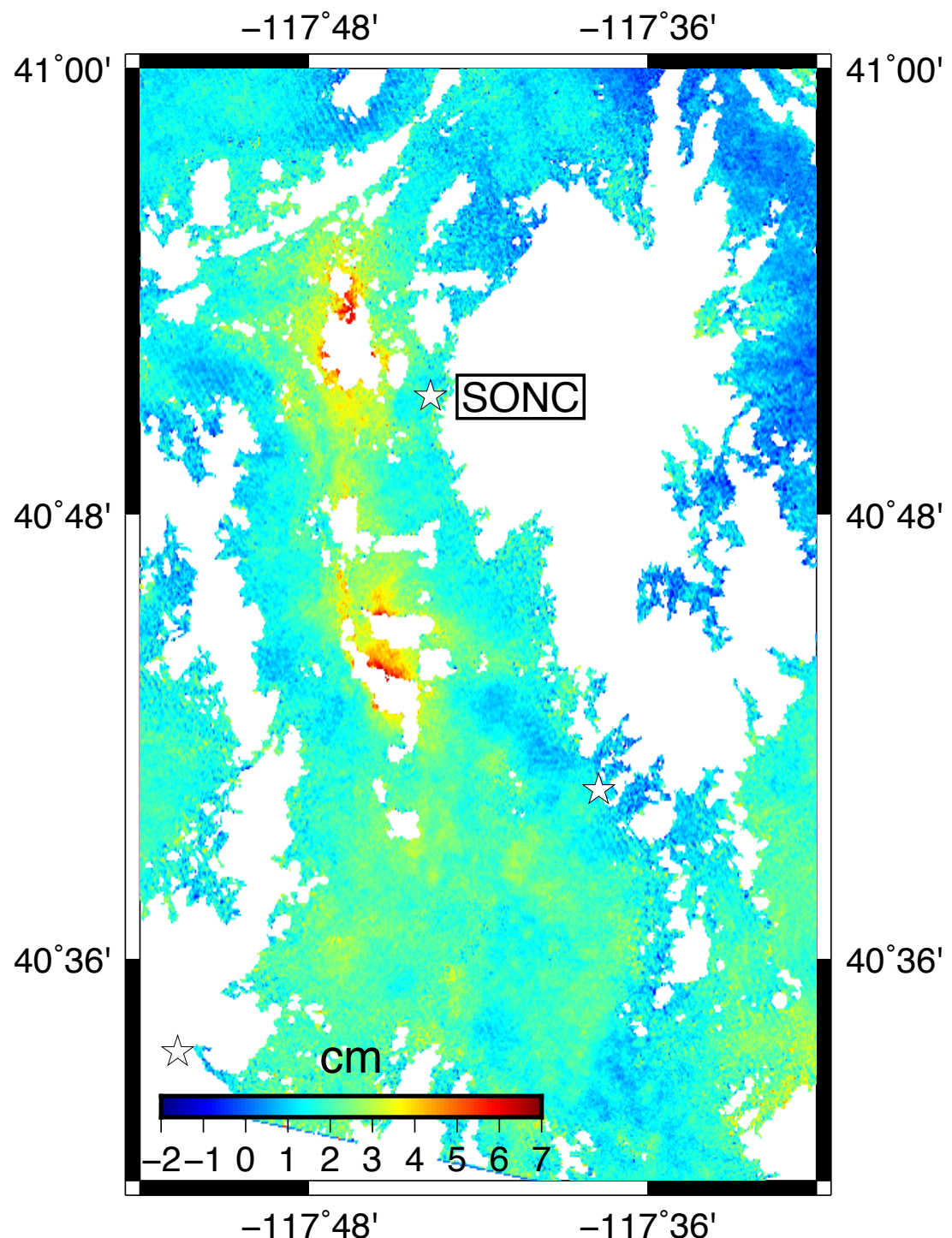
SUPPLEMENTAL FIGURE 29. Interferogram of fields east of Osgood Mountain, NV from Envisat spanning 23 Sept. 2008 - 6 May 2008. Stars indicate location of GPS sites.



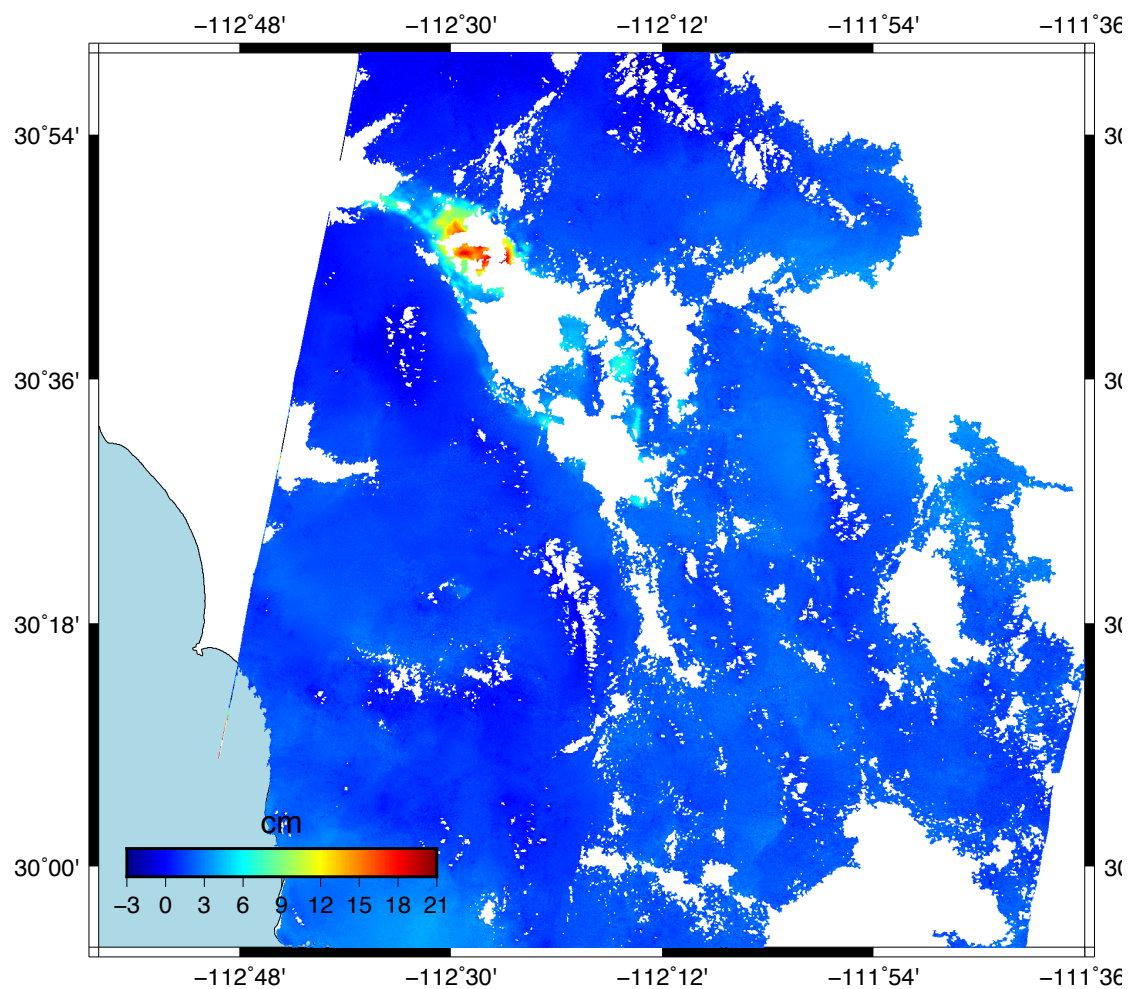
SUPPLEMENTAL FIGURE 30. Interferogram of fields south of Flowell, UT from Envisat spanning 7 Aug. 2008 - 20 March 2008.



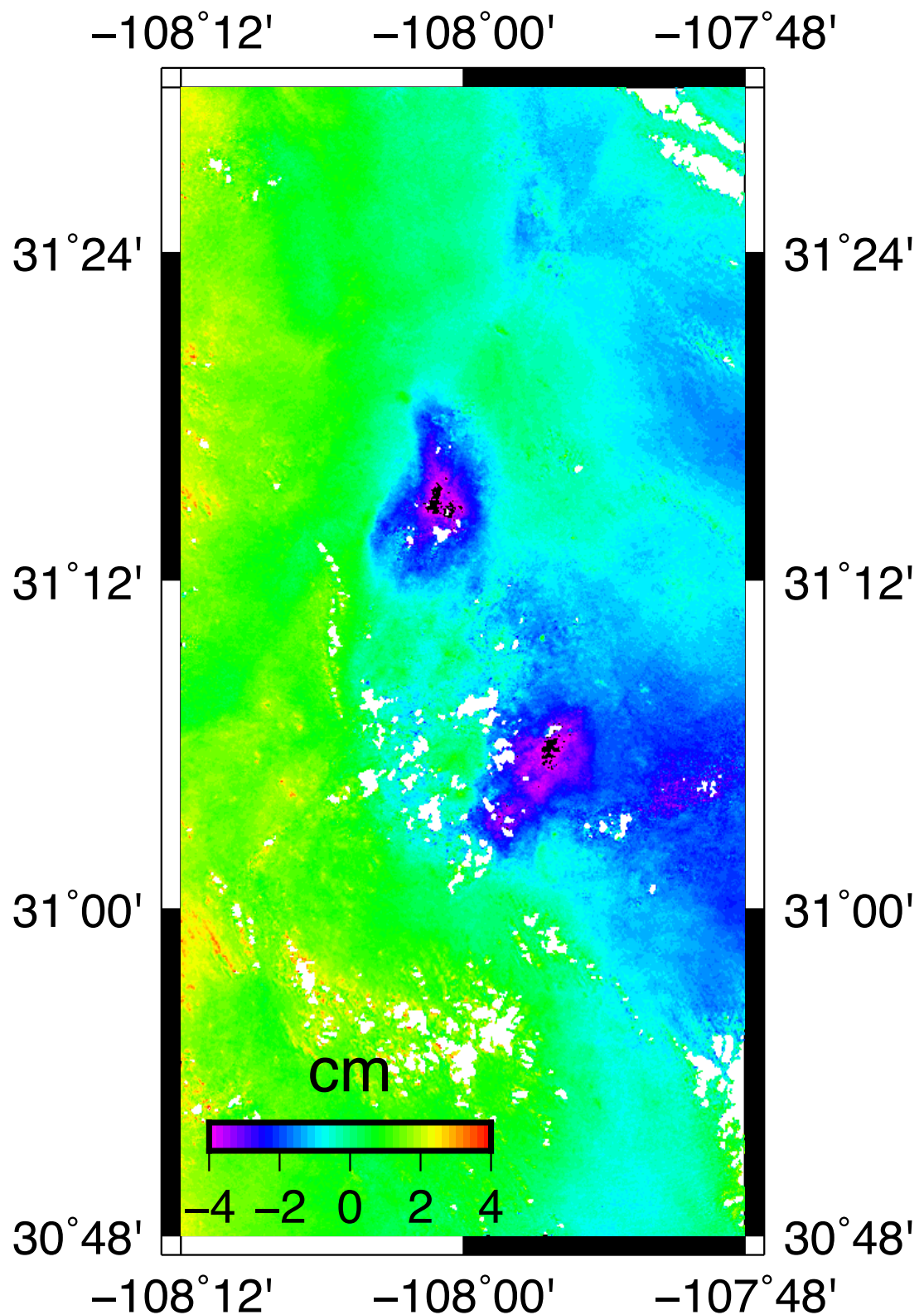
SUPPLEMENTAL FIGURE 31. Interferogram of fields west of Utah Lake, UT from Envisat spanning 18 Feb. 2010 - 23 July 2009.



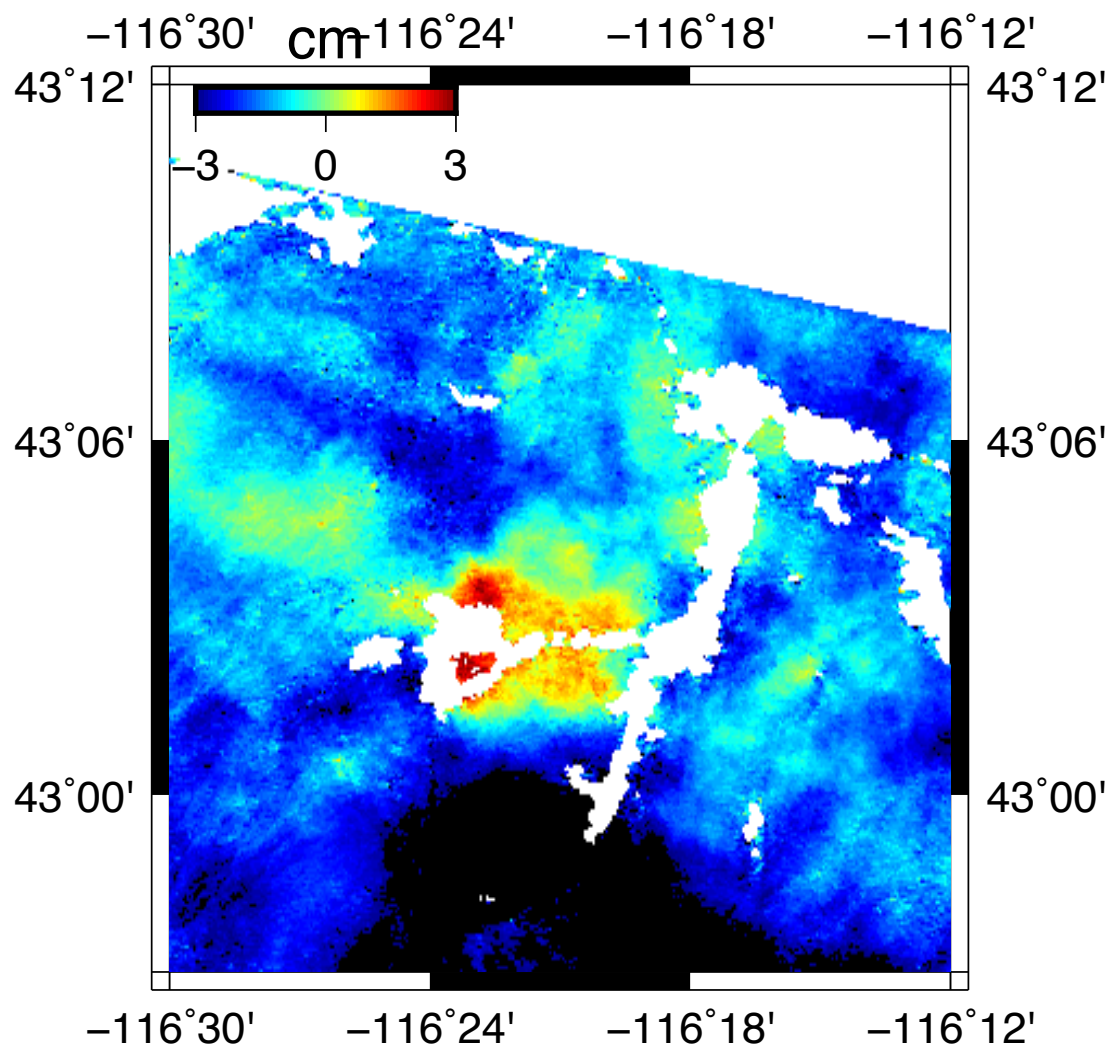
SUPPLEMENTAL FIGURE 32. Interferogram of Grass Valley, NV from Envisat spanning 23 Sept. 2008 - 26 June 2007. Stars indicate location of GPS sites – site SONC is potentially affected.



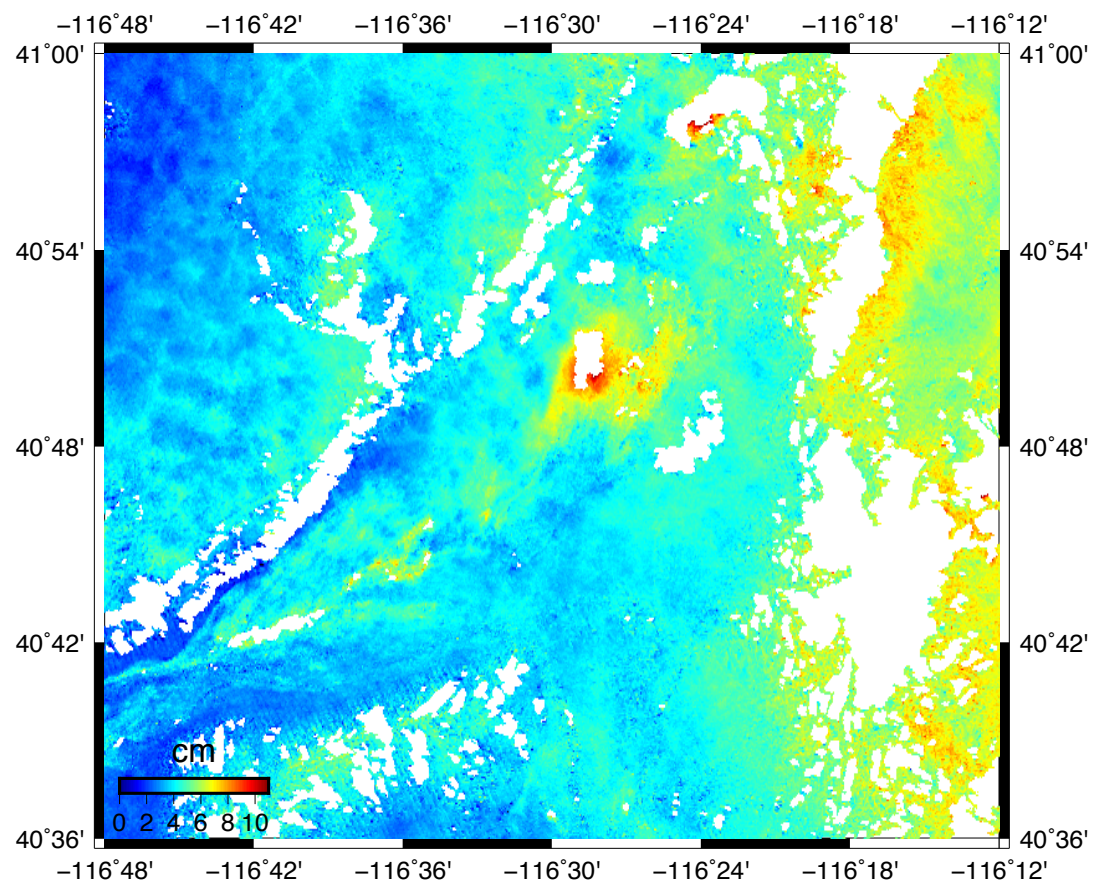
SUPPLEMENTAL FIGURE 33. Interferogram of Jesus Garcia, Mexico from Envisat spanning 11 Feb. 2009 - 7 Feb. 2007.



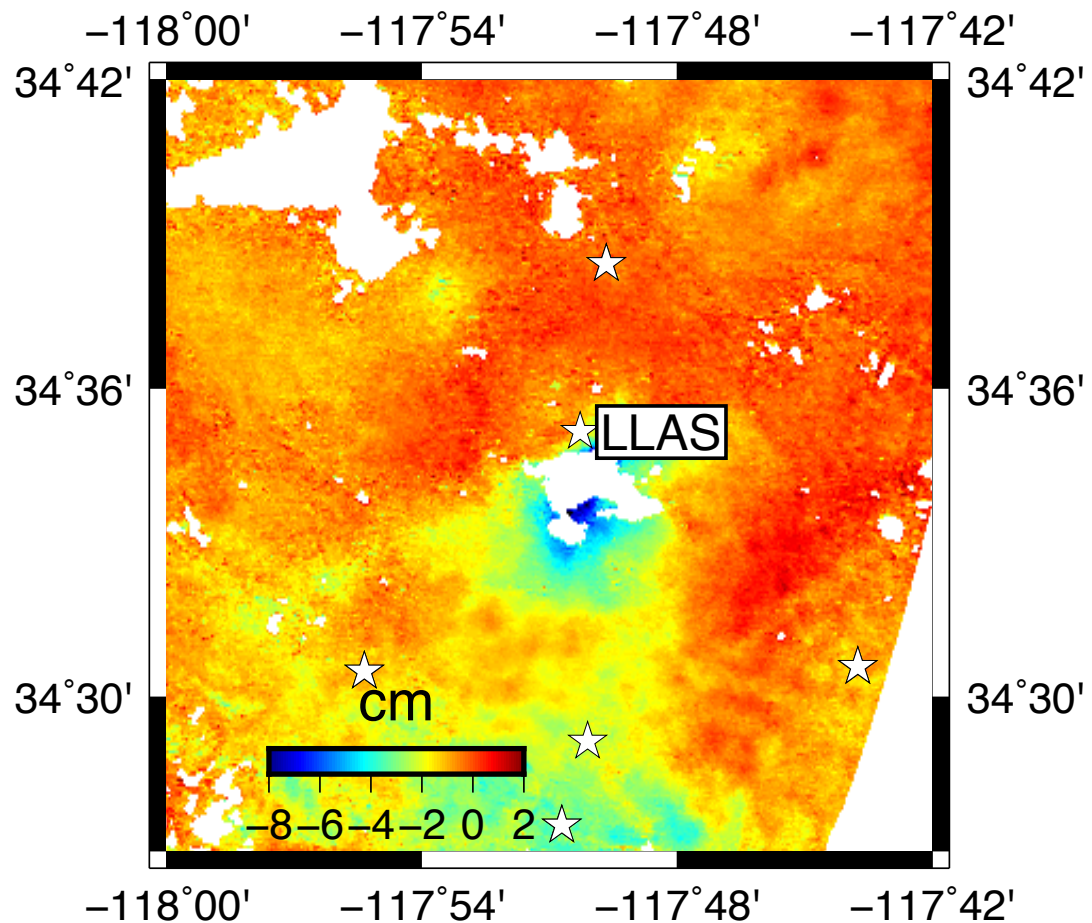
SUPPLEMENTAL FIGURE 34. Interferogram of South Espia and Asension, Mexico from ERS spanning 21 Jan. 1996 - 12 Nov. 1995.



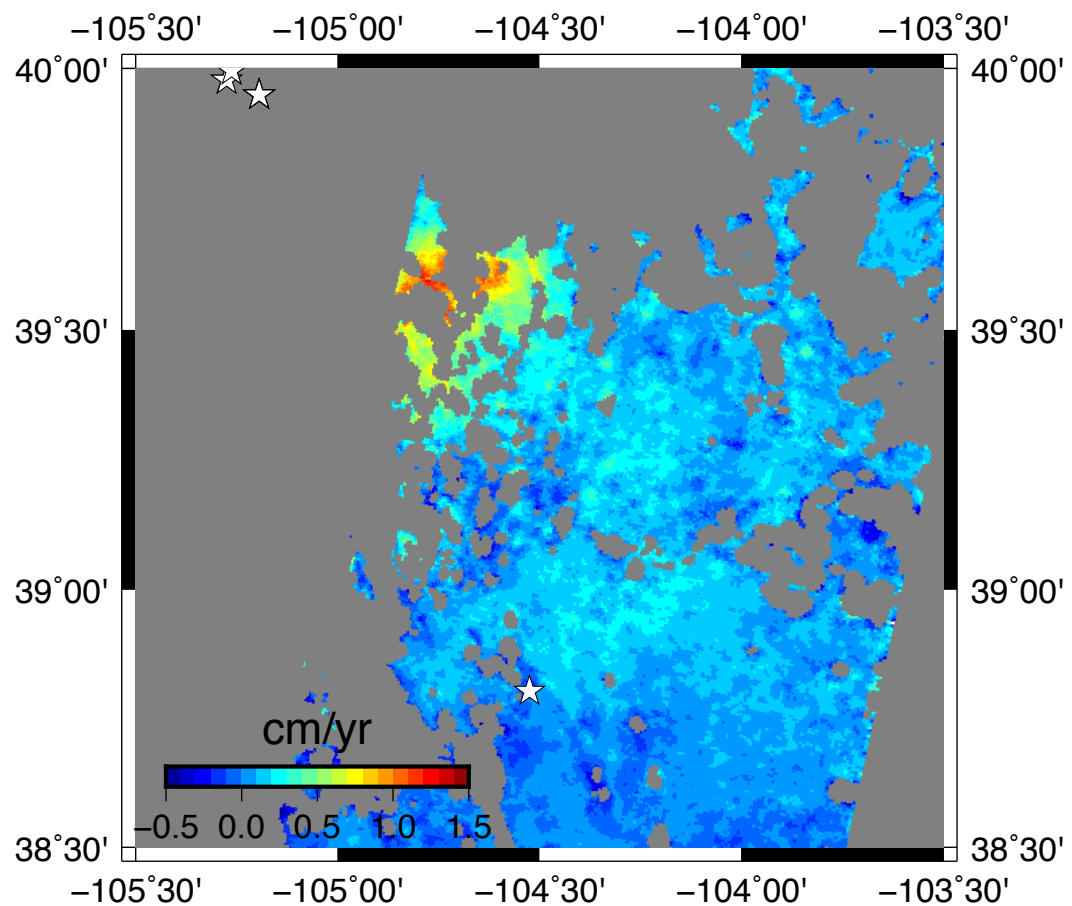
SUPPLEMENTAL FIGURE 35. Interferogram of Oreana, ID from Envisat spanning 10 June 2008 - 2 May 2006.



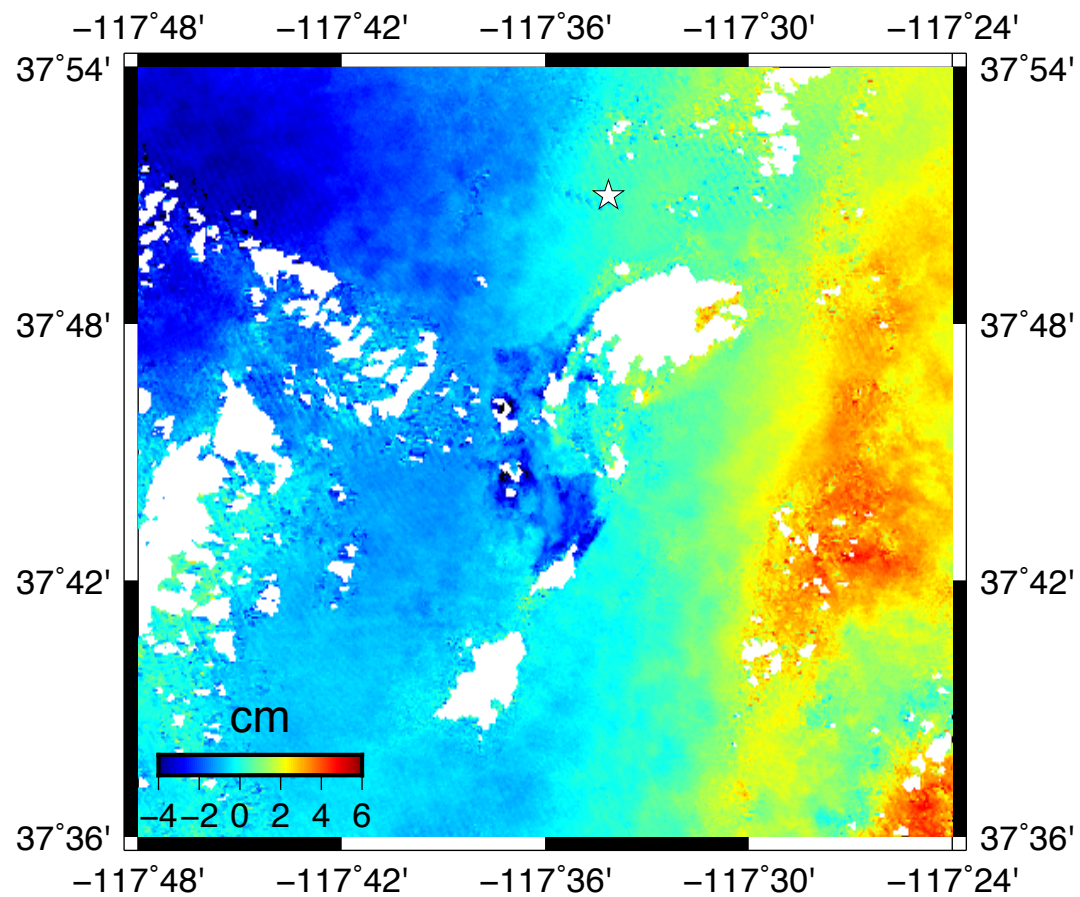
SUPPLEMENTAL FIGURE 36. Interferogram of agricultural fields south Goldstrike, NV from Envisat spanning 4 Sept. 2008 - 26 June 2008.



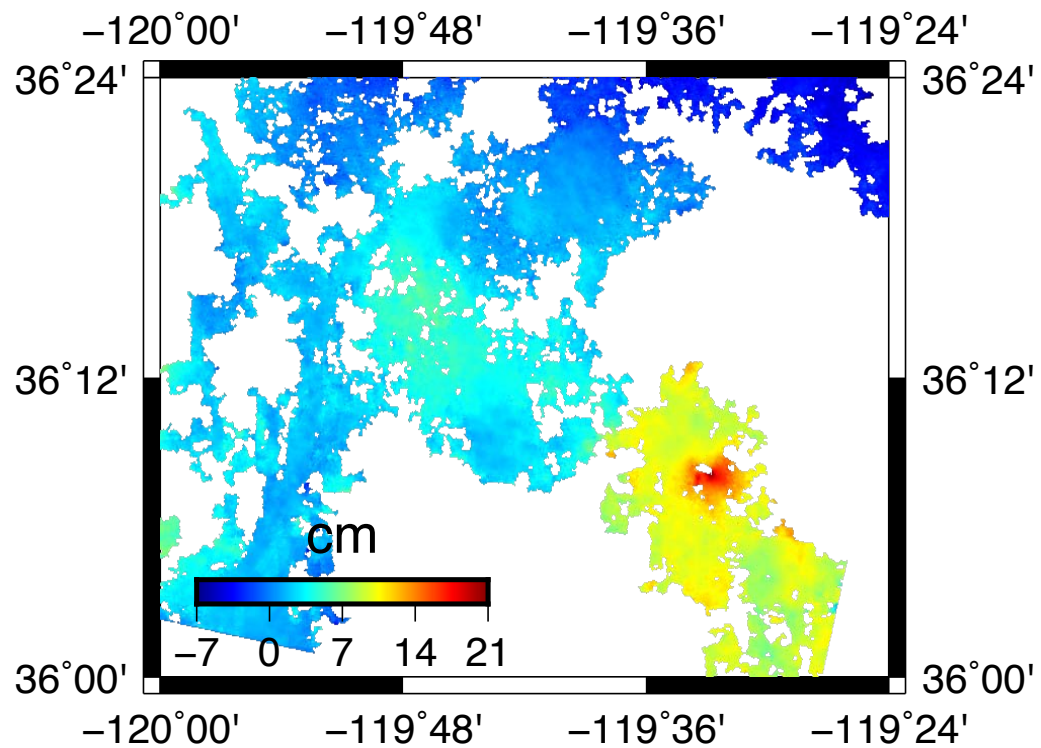
SUPPLEMENTAL FIGURE 37. Interferogram of agricultural fields south of Lake Los Angeles, CA from Envisat spanning 18 March 2010 - 4 Sept. 2008. Stars indicate location of GPS sites – site LLAS could be affected.



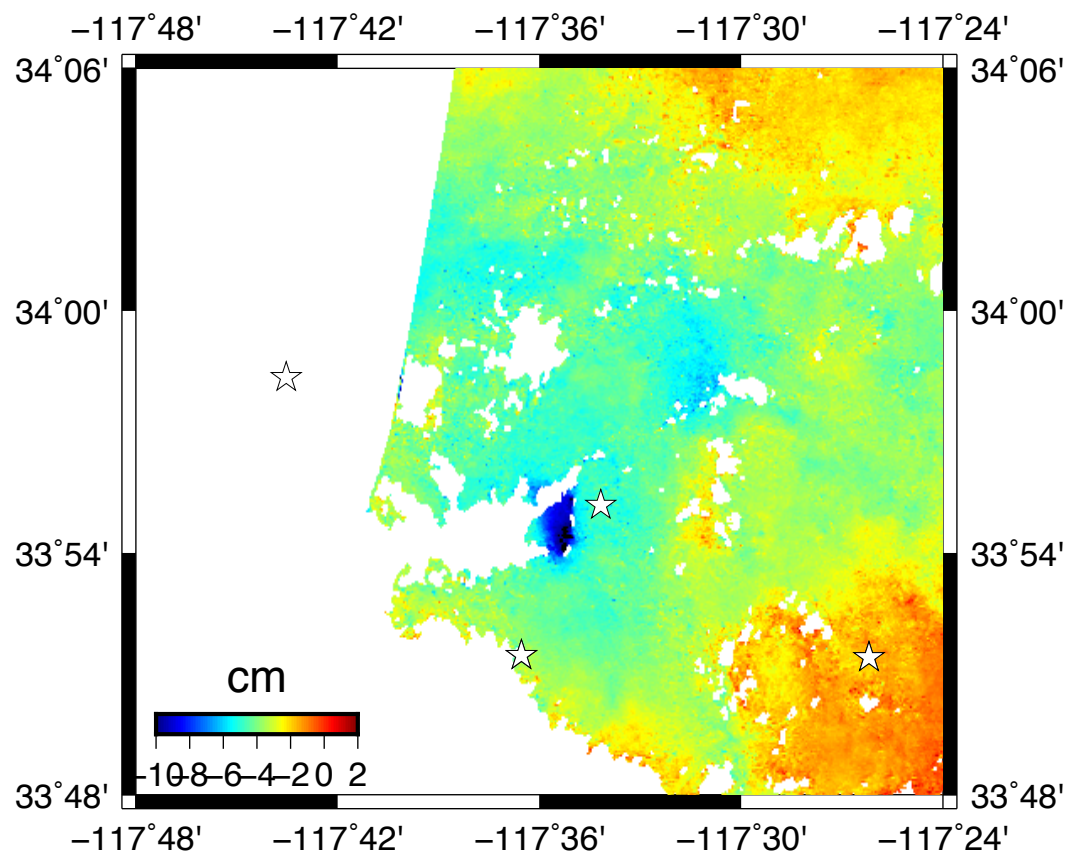
SUPPLEMENTAL FIGURE 38. Interferogram of Centennial, CO time series from ERS spanning 9 June 1992 - 3 Nov. 2000. Stars indicate location of GPS sites.



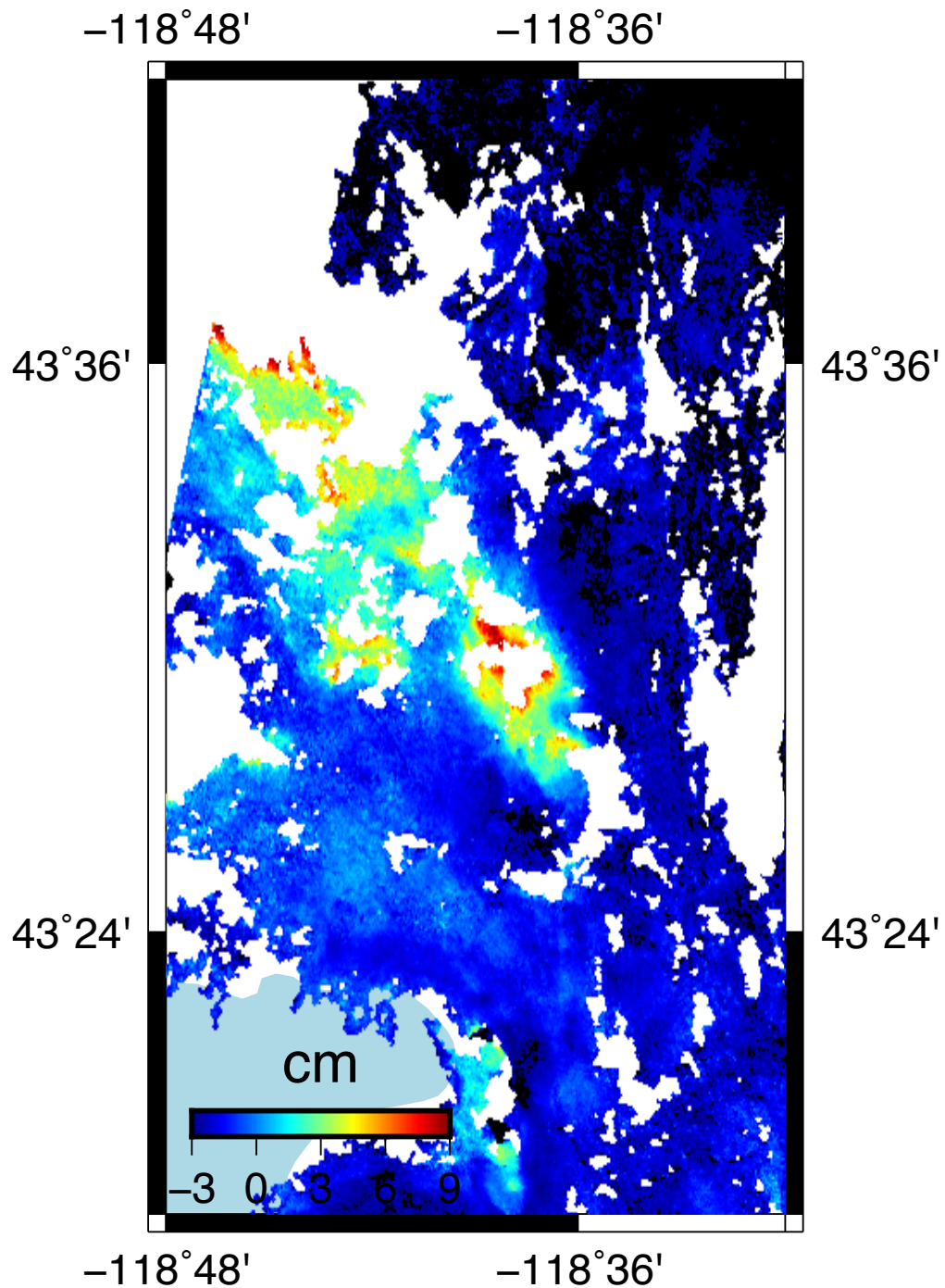
SUPPLEMENTAL FIGURE 39. Interferogram near Chemetall Foote Lithium Operation, CA from Envisat spanning 4 Sept. 2008 - 26 June 2008. Stars indicate location of GPS sites.



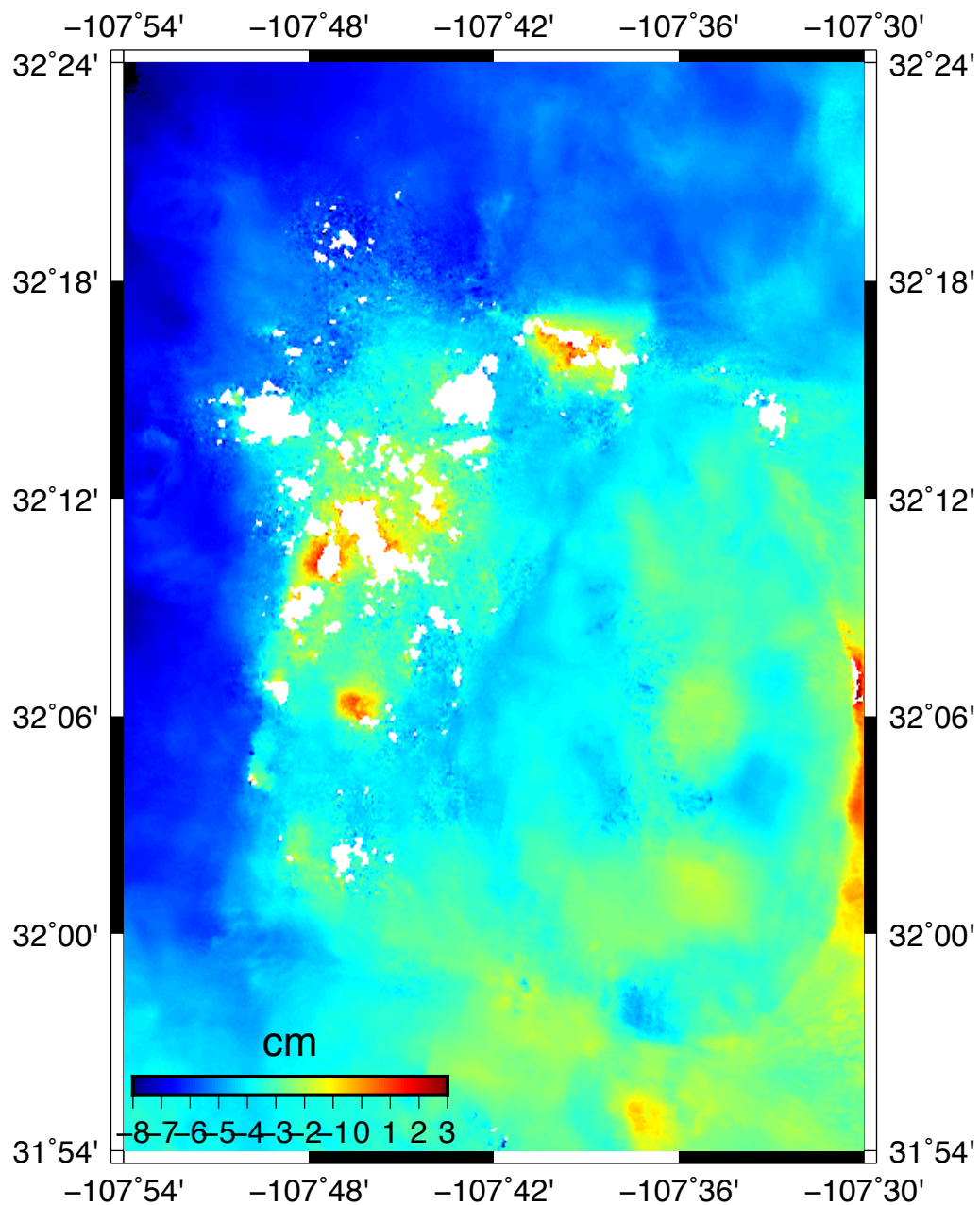
SUPPLEMENTAL FIGURE 40. Interferogram of Corcoran, CA from Envisat spanning 13 June 2008 - 9 May 2008.



SUPPLEMENTAL FIGURE 41. Interferogram of Corona, CA from Envisat spanning 26 Nov. 2007 - 17 Sept. 2007. Stars indicate location of GPS sites.



SUPPLEMENTAL FIGURE 42. Interferogram of Crane, OR from Envisat spanning 1 Oct. 2010 - 9 Apr. 2010.



SUPPLEMENTAL FIGURE 43. Interferogram of Deming, NM from Envisat spanning 7 June 2010 - 18 Jan. 2010.

61

REFERENCES

- 62 ADWR, Arizona department of water resources, land subsidence in Arizona, 2015,
63 retrieved April 8, 2015.
- 64 Ali, S. T., N. C. Davatzes, K. L. Feigl, H. F. Wang, W. Foxall, R. J. Mellors, J. Ak-
65 erley, E. Zemach, and P. Spielman, Deformation at Brady Hot Springs geother-
66 mal field measured by time series analysis of InSAR data, in *PROCEEDINGS,*
67 *Fourtieth Workshop on Geothermal Reservoir Engineering Stanford University,*
68 *Stanford, California*, vol. 40, pp. 26–28, 2015.
- 69 Ali, S. T., J. Akerley, E. C. Baluyut, N. C. Davatzes, J. Lopeman, J. Moore, M. Plum-
70 mer, P. Spielman, I. Warren, and K. L. Feigl, Geodetic measurements and numeri-
71 cal models of deformation: Examples from geothermal fields in the western United
72 States, in *PROCEEDINGS, 41st Workshop on Geothermal Reservoir Engineer-*
73 *ing Stanford University, Stanford, California, February 22-24, 2016 SGP-TR-209,*
74 2016.
- 75 Amelung, F., D. Galloway, J. Bell, H. Zebker, and R. Lacznak, Sensing the ups
76 and downs of Las Vegas: InSAR reveals structural control of land subsidence and
77 aquifer-system deformation, *Geology*, 27, 483–486, 1999.
- 78 Arai, R., Application of synthetic aperture radar interferometry (InSAR) in defining
79 groundwater-withdrawal-related subsidence, Diamond Valley, Nevada, Master's
80 thesis, University of Nevada, Reno, 2009.
- 81 Argus, D. F., M. B. Heflin, G. Peltzer, F. Crampé, and F. H. Webb, Interseismic
82 strain accumulation and anthropogenic motion in metropolitan Los Angeles, *Jour-*
83 *nal of Geophysical Research: Solid Earth*, 110, 2005.
- 84 Arroyo, M., J. Arzate, V. Yutsis, and J. Martínez, Estudio integral del recurso agua
85 en los acuíferos del estado de Querétaro, área de geofísica, geología y geotécnia,
86 *Reporte Comisión Estatal de Agua (CEA), Querétaro, México*, 2002.

- 87 Baek, J., S.-W. Kim, and J. W. Kim, Monitoring of ground surface and subsurface
88 deformations at oil sands using radar interferometry, *Geophysics*, **80**, EN137–
89 EN152, 2015.
- 90 Barnhart, W. D., H. M. Benz, G. P. Hayes, J. L. Rubinstein, and E. Bergman,
91 Seismological and geodetic constraints on the 2011 M_w 5.3 Trinidad, Colorado
92 earthquake and induced deformation in the Raton Basin, *Journal of Geophysical
93 Research: Solid Earth*, **119**, 7923–7933, 2014.
- 94 Bawden, G. W., W. Thatcher, R. S. Stein, K. W. Hudnut, and G. Peltzer, Tectonic
95 contraction across Los Angeles after removal of groundwater pumping effects, *Nature*,
96 **412**, 812 – 815, 2001.
- 97 Bekaert, D., B. Hamlington, B. Buzzanga, and C. Jones, Spaceborne Synthetic Aper-
98 ture Radar survey of subsidence in Hampton Roads, Virginia (USA), *Scientific
99 Reports*, **7**, 14,752, 2017.
- 100 Bell, J. W., G. L. Oppliger, and K. Katzenstein, InSAR across the Sierra Nevada-
101 Basin and Range transition zone, *Final Technical Report, USGS NEHRP program*,
102 2008, [Date accessed: May 26, 2017].
- 103 Blodgett, J., M. Ikehara, and G. Williams, Monitoring land subsidence in Sacramento
104 Valley, California, using GPS, *Journal of Surveying Engineering*, **116**, 112–130,
105 1990.
- 106 Brunori, C. A., C. Bignami, M. Albano, F. Zucca, S. Samsonov, G. Groppelli,
107 G. Norini, M. Saroli, and S. Stramondo, Land subsidence, ground fissures and
108 buried faults: InSAR monitoring of Ciudad Guzmán (Jalisco, Mexico), *Remote
109 Sensing*, **7**, 8610–8630, 2015.
- 110 Buckley, S. M., P. A. Rosen, S. Hensley, and B. D. Tapley, Land subsidence in Hous-
111 ton, Texas, measured by radar interferometry and constrained by extensometers,
112 *Journal of Geophysical Research: Solid Earth (1978–2012)*, **108**, 2003.

- 113 Cabral-Cano, E., T. H. Dixon, F. Miralles-Wilhelm, O. Díaz-Molina, O. Sánchez-
114 Zamora, and R. E. Carande, Space geodetic imaging of rapid ground subsidence
115 in Mexico City, *Geological Society of America Bulletin*, 120, 1556–1566, 2008.
- 116 Carnec, C., and H. Fabriol, Monitoring and modeling land subsidence at the Cerro
117 Prieto geothermal field, Baja California, Mexico, using SAR interferometry, *Geo-
118 physical Research Letters*, 26, 1211–1214, 1999.
- 119 Casu, F., M. Manzo, A. Pepe, and R. Lanari, SBAS-DInSAR analysis of very ex-
120 tended areas: First results on a 60,000-test site, *Geoscience and Remote Sensing
121 Letters, IEEE*, 5, 438–442, 2008.
- 122 Cavalié, O., M.-P. Doin, C. Lasserre, and P. Briole, Ground motion measurement in
123 the Lake Mead area, Nevada, by differential synthetic aperture radar interferome-
124 try time series analysis: Probing the lithosphere rheological structure, *Journal of
125 Geophysical Research: Solid Earth (1978–2012)*, 112, 2007.
- 126 Chaussard, E., S. Wdowinski, E. Cabral-Cano, and F. Amelung, Land subsidence in
127 central Mexico detected by ALOS InSAR time-series, *Remote sensing of environ-
128 ment*, 140, 94–106, 2014.
- 129 Cigna, F., B. Osmanoğlu, E. Cabral-Cano, T. H. Dixon, J. A. Ávila-Olivera, V. H.
130 Garduño-Monroy, C. DeMets, and S. Wdowinski, Monitoring land subsidence and
131 its induced geological hazard with synthetic aperture radar interferometry: A case
132 study in Morelia, Mexico, *Remote Sensing of Environment*, 117, 146–161, 2012.
- 133 Coyne, J. M., New estimates of crustal motion in the western United States, Master's
134 thesis, Cornell University, 1988.
- 135 Densmore, J., K. Ellett, J. Howle, M. Carpenter, and M. Sneed, Monitoring land-
136 surface deformation on Bicycle Lake playa, Fort Irwin, California, USA, *IAHS-AISH
137 publication*, pp. 39–43, 2010.
- 138 Dixon, T. H., F. Amelung, A. Ferretti, F. Novali, F. Rocca, R. Dokka, G. Sella, S.-W.
139 Kim, S. Wdowinski, and D. Whitman, Space geodesy: Subsidence and flooding in

- 140 New Orleans, *Nature*, 441, 587–588, 2006.
- 141 142 143 144 Donovan, J., F. Ismaya, et al., Case study: Measuring subsidence above coal mines using differential interferometric synthetic aperture radar, in *44th US Rock Mechanics Symposium and 5th US-Canada Rock Mechanics Symposium*, American Rock Mechanics Association, 2010.
- 145 146 147 148 Eneva, M., G. Falorni, W. Teplow, J. Morgan, G. Rhodes, and D. Adams, Surface deformation at the San Emidio Geothermal Field, Nevada, from satellite radar interferometry, in *Geoth. Resour. Counc.-Trans*, vol. 35, p. 1647=1653, 2011, [Date accessed: May 26, 2017].
- 149 150 151 Eneva, M., D. Adams, G. Falorni, and J. Morgan, Surface deformation in Imperial Valley, CA, from satellite radar interferometry, in *Geoth. Resour. Counc.-Trans*, vol. 36, pp. 1339–1344, 2012.
- 152 153 154 Farr, T. G., InSAR measurements of subsidence in the Central Valley, California from 2007-present, in *EUSAR 2016: 11th European Conference on Synthetic Aperture Radar, Proceedings of*, pp. 1–3, VDE, 2016.
- 155 156 157 Fialko, Y., and M. Simons, Deformation and seismicity in the Coso geothermal area, Inyo County, California: Observations and modeling using satellite radar interferometry, *Journal of Geophysical Research B*, 105, 21,781–21,793, 2000.
- 158 159 Fielding, E. J., R. G. Blom, and R. M. Goldstein, Rapid subsidence over oil fields measured by SAR interferometry, *Geophys. Res. Lett.*, 25, 3215–3218, 1998.
- 160 161 162 Finnegan, N. J., M. E. Pritchard, R. B. Lohman, and P. R. Lundgren, Constraints on surface deformation in the Seattle, WA urban corridor from satellite radar interferometry time series analysis,, *Geophys. J. Int.*, 174, 29–41, 2008.
- 163 164 165 Forster, R. R., *Land Subsidence in Southwest Utah from 1993 to 1996 Measured with Interferometric Synthetic Aperture Radar (InSAR)*, volume 6, Utah Geological Survey, 2006.

- 166 Foxall, B., and D. Vasco, Inversion of synthetic aperture radar interferograms for
167 sources of production-related subsidence at the Dixie Valley geothermal field,
168 *Lawrence Berkeley National Laboratory*, 2008.
- 169 Galloway, D. L., K. Hudnut, S. Ingebritsen, S. Phillips, G. Peltzer, F. Rogez, and
170 P. Rosen, Detection of aquifer system compaction and land subsidence using inter-
171 ferometric synthetic aperture radar, Antelope Valley, Mojave Desert, California,
172 *Water Resources Research*, 34, 2573–2585, 1998.
- 173 Gourmelen, N., F. Amelung, F. Casu, M. Manzo, and R. Lanari, Mining-related
174 ground deformation in Crescent Valley, Nevada: Implications for sparse GPS net-
175 works, *Geophysical Research Letters*, 34, 2007.
- 176 Gourmelen, N., F. Amelung, and R. Lanari, Interferometric synthetic aperture radar–
177 GPS integration: Interseismic strain accumulation across the Hunter Mountain
178 fault in the eastern California shear zone, *Journal of Geophysical Research: Solid*
179 *Earth (1978–2012)*, 115, 2010.
- 180 Greene, F., Surface deformation measured with interferometric synthetic aperture
181 radar: Case studies of Basin and Range and Garlock-San Andreas Fault, Ph.D.
182 thesis, University of Miami, 2014.
- 183 Grigg, K. M., and K. W. Katzenstein, Using InSAR and groundwater pumping data
184 to model land subsidence from coalbed methane production in the Powder River
185 Basin, Wyoming, in *2013 GSA Annual Meeting in Denver*, 2013.
- 186 Grzovic, M., and A. Ghulam, Evaluation of land subsidence from underground coal
187 mining using TimeSAR (SBAS and PSI) in Springfield, Illinois, USA, *Natural*
188 *Hazards*, 79, 1739–1751, 2015.
- 189 Hammond, W. C., and J. W. Bell, Structural controls on geothermal reservoir de-
190 formation at Stillwater, Nevada from InSAR and GPS data, *GRC Transactions*,
191 37, 11–15, 2013.

- 192 Han, J. Y., R. R. Forster, D. E. Moser, A. L. J. Ford, J. Ramírez-Hernández, and
193 K. F. Tiampo, The spatial and temporal subsidence variability of the East Mesa
194 Geothermal Field, California, USA, and its potential impact on the all American
195 canal system, *International journal of remote sensing*, 32, 3427–3449, 2011.
- 196 Heywood, C. E., D. L. Galloway, and S. V. Stork, Ground displacements caused
197 by aquifer-system water-level variations observed using interferometric synthetic
198 aperture radar near Albuquerque, New Mexico, 2002.
- 199 Hoppe, E., A. Bohane, G. Falorni, B. Bruckno, A. Vaccari, F. Meyer, and
200 M. Pritchard, InSAR remote sensing for performance monitoring of transporta-
201 tion infrastructure at the network level, in *Transport Research Arena TRA2016*,
202 Warsaw, Poland, 2016.
- 203 Hsiao, V., Practical examples of InSAR monitoring, in *Using Interferometric syn-
204 thetic aperture radar for network-wide transportation infrastructure monitoring*,
205 *Transportation Resaerch Board webinar*, The National Academies of Science, En-
206 gineering, and Medicine, 2016.
- 207 Ikebara, M. E., Global positioning system surveying to monitor land subsidence in
208 Sacramento Valley, California, USA, *Hydrological sciences journal*, 39, 417–429,
209 1994.
- 210 Ireland, R. L., J. F. Poland, and F. S. Riley, *Land subsidence in the San Joaquin
211 Valley, California, as of 1980*, US Government Printing Office, 1984.
- 212 Ismaya, F., and J. Donovan, Applications of DInSAR for measuring mine-induced
213 subsidence and constraining ground deformation model, *GeoCongress 2012 State
214 of the Art and Practice in Geotechnical Engineering*, 25-29 March 2012, pp. 3001–
215 10, 2012.
- 216 Jones, C. E., and R. G. Blom, Bayou Corne, Louisiana, sinkhole: Precursory defor-
217 mation measured by radar interferometry, *Geology*, 42, 111–114, 2014.

- 218 Karegar, M. A., T. H. Dixon, R. Malservisi, Q. Yang, S. A. Hossaini, and S. D.
219 Hovorka, GPS-based monitoring of surface deformation associated with CO_2 in-
220 jection at an enhanced oil recovery site, *International Journal of Greenhouse Gas
Control*, 41, 116–126, 2015.
- 222 Katzenstein, K. W., Mechanics of InSAR-identified bedrock subsidence associated
223 with mine-dewatering in north-central Nevada, Ph.D. thesis, University of Nevada,
224 Reno, 2008.
- 225 Khakim, M. Y. N., T. Tsuji, and T. Matsuoka, Detection of localized surface uplift
226 by differential SAR interferometry at the Hangingstone oil sand field, Alberta,
227 Canada, *Selected Topics in Applied Earth Observations and Remote Sensing, IEEE
Journal of*, 6, 2344–2354, 2013.
- 229 King, N., D. Argus, J. Langbein, D. Agnew, G. Bawden, R. Dollar, Z. Liu, D. Gal-
230 loway, E. Reichard, A. Yong, et al., Space geodetic observation of expansion of
231 the San Gabriel Valley, California, aquifer system, during heavy rainfall in winter
232 2004–2005, *Journal of Geophysical Research: Solid Earth (1978–2012)*, 112, 2007.
- 233 Knudsen, T., P. Inkenbrandt, W. Lund, M. Lowe, and S. Bowman, *Investigation of
land subsidence and earth fissures in Cedar Valley, Iron County, Utah*, vol. 150,
235 Utah Geological Survey, 2014.
- 236 Lofgren, B. E., Land subsidence and tectonism, Raft River Valley, Idaho, *Geol. Surv.,
Open-File Rep. 75-585*, p. 21, 1975.
- 238 López-Doncel, R., J. L. Mata-Segura, J. Cruz-Márquez, J. Arzate-Flores, and
239 J. Pacheco-Martínez, Riesgo geológico para el patrimonio histórico. Ejemplos del
240 centro histórico de la ciudad de San Luis Potosí, *Boletín de la Sociedad Geológica
Mexicana*, 58, 259–263, 2006.
- 242 Lund, W., C. DuRoss, S. Kirby, G. McDonald, G. Hunt, and G. Vice, The origin
243 and extent of earth fissures in Escalante Valley, southern Escalante Desert, *Iron
County, Utah: Utah Geological Survey Special Study*, 115, 30, 2005.

- 245 Marshall, S. T., G. J. Funning, and S. E. Owen, Fault slip rates and interseismic
246 deformation in the western Transverse Ranges, California, *Journal of Geophysical*
247 *Research: Solid Earth*, *118*, 4511–4534, 2013.
- 248 Massonnet, D., T. Holzer, and H. Vadon, Land subsidence caused by the East Mesa
249 geothermal field, California, observed using SAR interferometry, *Geophysical Re-*
250 *search Letters*, *24*, 901–904, 1997.
- 251 Mata-Segura, J., R. López-Doncel, R. Rodríguez-Ríos, J. Arzate-Flores, and
252 J. Pacheco-Martínez, Problemática de las fallas geológicas en la zona urbana y
253 conurbada de San Luis Potosí-Soledad de Graciano Sánchez (resumen), *IV Re-*
254 *unión Nacional de Ciencias de la Tierra, Juriquilla, Qro*, *87*, 2004.
- 255 Mazzotti, S., A. Lambert, M. Van der Kooij, and A. Mainville, Impact of anthro-
256 pogenic subsidence on relative sea-level rise in the Fraser River delta, *Geology*, *37*,
257 771–774, 2009.
- 258 Mei, S., V. Poncos, and C. Froese, Mapping millimetre-scale ground deformation
259 over the underground coal mines in the Frank Slide area, Alberta, Canada, using
260 spaceborne InSAR technology, *Canadian Journal of Remote Sensing*, *34*, 113–134,
261 2008.
- 262 Miller, M. M., and M. Shirzaei, Spatiotemporal characterization of land subsidence
263 and uplift in Phoenix using InSAR time series and wavelet transforms, *Journal of*
264 *Geophysical Research: Solid Earth*, *120*, 5822–5842, 2015.
- 265 Osmanoğlu, B., T. H. Dixon, S. Wdowinski, E. Cabral-Cano, and Y. Jiang, Mexico
266 City subsidence observed with persistent scatterer InSAR, *International Journal*
267 *of Applied Earth Observation and Geoinformation*, *13*, 1–12, 2011.
- 268 Pacheco, J., J. Arzate, E. Rojas, M. Arroyo, V. Yutsis, and G. Ochoa, Delimitation
269 of ground failure zones due to land subsidence using gravity data and finite element
270 modeling in the Querétaro valley, México, *Engineering Geology*, *84*, 143–160, 2006.

- 271 Pavelko, M. T., D. B. Wood, and R. J. Lacniak, Las Vegas, Nevada, *Land subsidence*
272 *in the United States: US Geological Survey Circular*, 1182, 49–64, 1999.
- 273 Pearse, J., V. Singhroy, S. Samsonov, and J. Li, Anomalous surface heave induced
274 by enhanced oil recovery in northern Alberta: InSAR observations and numerical
275 modeling, *Journal of Geophysical Research: Solid Earth*, 119, 6630–6649, 2014.
- 276 Plattner, C., S. Wdowinski, T. H. Dixon, and J. Biggs, Surface subsidence induced by
277 the Crandall Canyon Mine (Utah) collapse: InSAR observations and elasto-plastic
278 modelling, *Geophysical Journal International*, 183, 1089–1096, 2010.
- 279 Pollack, A., R. Munda, T. Farrell, S. Kelley, J. Frost, and G. Jiracek, Anomalously
280 high geothermal gradients in the Buckman Well Field, Santa Fe County, New
281 Mexico, in *AGU Fall Meeting Abstracts*, vol. 1, p. 1228, 2013.
- 282 Prush, V. B., and R. B. Lohman, Time-varying elevation change at the Centralia
283 Coal Mine in Centralia, Washington (USA), constrained with InSAR, ASTER, and
284 optical imagery, *IEEE Journal of Selected Topics in Applied Earth Observations*
285 and *Remote Sensing*, 8, 919–925, 2015.
- 286 Reeves, J. A., R. Knight, H. A. Zebker, W. A. Schreüder, P. Shanker Agram, and
287 T. R. Lauknes, High quality InSAR data linked to seasonal change in hydraulic
288 head for an agricultural area in the San Luis Valley, Colorado, *Water Resources*
289 *Research*, 47, 2011.
- 290 Samsonov, S., P. J. Gonzalez, K. Tiampo, and N. d'Oreye, Spatio-temporal analysis
291 of ground deformation occurring near Rice Lake, Saskatchewan, and observed by
292 Radarsat-2 DInSAR during 2008–2011, *Canadian Journal of Remote Sensing*, 39,
293 27–33, 2013.
- 294 Samsonov, S., P. González, K. Tiampo, and N. d'Oreye, Modeling of fast ground sub-
295 sidence observed in southern Saskatchewan (Canada) during 2008–2011, *Natural*
296 *Hazards and Earth System Science*, 14, 247–257, 2014.

- 297 Samsonov, S., M. Czarnogorska, and D. White, Satellite interferometry for high-
298 precision detection of ground deformation at a carbon dioxide storage site, *International
299 Journal of Greenhouse Gas Control*, 42, 188–199, 2015.
- 300 Sarychikhina, O., E. Glowacka, R. Mellors, and F. S. Vidal, Land subsidence in the
301 Cerro Prieto Geothermal Field, Baja California, Mexico, from 1994 to 2005: An
302 integrated analysis of DInSAR, leveling and geological data, *Journal of Volcanology
303 and Geothermal Research*, 204, 76–90, 2011.
- 304 Schmidt, D. A., and R. Bürgmann, Time-dependent land uplift and subsidence in
305 the Santa Clara valley, California, from a large interferometric synthetic aperture
306 radar data set, *J. Geophys. Res.*, 108, 10.1029/2002JB002,267, 2003.
- 307 Semmens, K. A., Mapping surface deformation associated with natural gas extraction
308 in the Powder River Basin, Wyoming determined using interferometric synthetic
309 aperture radar, in *2012 GSA Annual Meeting in Charlotte*, 2012.
- 310 Shevenell, L., G. Oppliger, M. Coolbaugh, and J. Faulds, Bradys (Nevada) InSAR
311 anomaly evaluated with historical well temperature and pressure data, *Geothermal
312 Resources Council Transactions*, 36, 1383–1390, 2012.
- 313 Sneed, M., and J. Brandt, *Detection and Measurement of Land Subsidence Us-
314 ing Global Positioning System Surveying and Interferometric Synthetic Aperture
315 Radar, Coachella Valley, California, 1996–2005*, 2013.
- 316 Sneed, M., M. E. Ikehara, S. V. Stork, F. Amelung, and D. L. Galloway, *Detection
317 and measurement of land subsidence using interferometric synthetic aperture radar
318 and global positioning system, San Bernardino County, Mojave Desert, California*,
319 US Department of the Interior, US Geological Survey, 2003.
- 320 Sneed, M., T. Nishikawa, and P. Martin, *Water Resources Investigations at Edwards
321 Air Force Base since 1988*, US Geological Survey, 2006.
- 322 Sneed, M., J. Brandt, and M. Solt, *Land subsidence along the Delta-Mendota Canal in
323 the northern part of the San Joaquin Valley, California, 2003-10*, US Department

- 324 of the Interior, US Geological Survey, 2013, [Date accessed: May 26, 2017].
- 325 Snieder, R., S. Hubbard, M. Haney, G. Bawden, P. Hatchell, A. Revil, D. G. M. W.
326 Group, et al., Advanced noninvasive geophysical monitoring techniques, *Annual
327 Review of Earth and Planetary Sciences*, *35*, 653, 2007.
- 328 Stancliffe, R. S., and M. W. van der Kooij, The use of satellite-based radar interfer-
329 ometry to monitor production activity at the Cold Lake heavy oil field, Alberta,
330 Canada, *AAPG bulletin*, *85*, 0781–0794, 2001.
- 331 Thomsen, D., and Y. Fialko, InSAR observed surface deformation at the Buckman
332 Well Field, New Mexico, in *AGU Fall Meeting Abstracts*, vol. 1, p. 0040, 2003.
- 333 Tibuleac, I., and M. Eneva, Seismic signature of the geothermal field at Soda Lake,
334 Nevada, from ambient noise analysis, *GRC Transactions*, *35*, 1767–1772, 2011.
- 335 Tizzani, P., P. Berardino, F. Casu, P. Euillades, M. Manzo, G. Ricciardi, G. Zeni, and
336 R. Lanari, Surface deformation of Long Valley caldera and Mono Basin, California,
337 investigated with the SBAS-InSAR approach, *Remote Sensing of Environment*,
338 *108*, 277–289, 2007.
- 339 USGS, and CGS, Quaternary fault and fold database for the United States, 2006,
340 retrieved January 9, 2016.
- 341 Valentine, D. W., J. N. Densmore, D. L. Galloway, and F. Amelung, *Use of InSAR
342 to identify land-surface displacements caused by aquifer-system compaction in the
343 Paso Robles Area, San Luis Obispo County, California, March to August 1997*,
344 US Geological Survey, 2000.
- 345 Valentino, B. R., Application of InSAR to salt mine subsidence, Master's thesis,
346 Cornell University, 2016, [Date accessed: May 26, 2017].
- 347 Vasco, D., J. Rutqvist, A. Ferretti, A. Rucci, F. Bellotti, P. Dobson, C. Oldenburg,
348 J. Garcia, M. Walters, and C. Hartline, Monitoring deformation at The Geysers
349 Geothermal Field, California using C-band and X-band interferometric synthetic
350 aperture radar, *Geophysical Research Letters*, *40*, 2567–2572, 2013.

- 351 Vincent, P., S. Larsen, D. Galloway, R. J. Laczniak, W. R. Walter, W. Foxall, and
352 J. J. Zucca, New signatures of underground nuclear tests revealed by satellite radar
353 interferometry, *Geophysical Research Letters*, 30, 2003.
- 354 Watson, K. M., Y. Bock, and D. T. Sandwell, Satellite interferometric observations
355 of displacements associated with seasonal groundwater in the Los Angeles basin,
356 *Journal of Geophysical Research: Solid Earth (1978–2012)*, 107, ETG–8, 2002.
- 357 Wicks, C. W., W. Thatcher, F. C. Monastero, and M. A. Hasting, Steady state
358 deformation of the Coso Range, east central California, inferred from satellite
359 radar interferometry, *Journal of Geophysical Research: Solid Earth (1978–2012)*,
360 106, 13,769–13,780, 2001.
- 361 Wynn, D., Geophysical monitoring of geologic sequestration in aquifers and depleted
362 oil and gas fields, Master's thesis, MS Thesis, Department of Geophysics, Stanford
363 University, 2003.
- 364 Yang, Q., W. Zhao, T. H. Dixon, F. Amelung, W. S. Han, and P. Li, InSAR mon-
365 itoring of ground deformation due to CO_2 injection at an enhanced oil recovery
366 site, West Texas, *International Journal of Greenhouse Gas Control*, 41, 20–28,
367 2015.
- 368 Zhao, W., F. Amelung, and T. Dixon, Monitoring ground deformation on carbon se-
369 questration reservoirs in North America, in *Fringe 2011 workshop, Frascati, Italy*,
370 vol. 697, 2012.